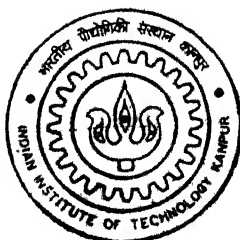


ELECTRICAL AND ELECTRIC MODULUS STUDIES ON $\text{Li}_3\text{PO}_4\text{-Li}_2\text{S}$ SUPERIONIC SYSTEM

by
Ashotosh Tiwari



TH
MS/2001/M
T543e

**MATERIALS SCIENCE PROGRAMME
INDIAN INSTITUTE OF TECHNOLOGY, KANPUR**

February, 2001

ELECTRICAL AND ELECTRIC MODULUS STUDIES ON $\text{Li}_3\text{PO}_4\text{-Li}_2\text{S}$ SUPERIONIC SYSTEM

*A thesis submitted in partial fulfillment of
the requirements for the degree of*

Master of Technology

by
Ashotosh Tiwari



**Materials Science Programme
INDIAN INSTITUTE OF TECHNOLOGY KANPUR**

February 2001

12/11/21/MS
विश्वविद्यालय
काठमाडौं काठमाडौं
अवधि-०९/133680



A133680

Certificate

28 2-01

12/2/01

It is certified that the work presented in this thesis entitled 'Electrical and Electric Modulus Studies on $\text{Li}_3\text{PO}_4\text{-Li}_2\text{S}$ Superionic System', by Ashotosh Tiwari, has been carried out under my supervision and that this work has not been submitted elsewhere for a degree

K. Shahi

(Prof. K. Shahi)

Thesis Supervisor

Materials Science Programme

IIT Kanpur

IIT Kanpur
February, 2001

Abstract

Different Compositions of $\text{Li}_3\text{PO}_4\text{-Li}_2\text{S}$ superionic systems have been investigated. Eight different compositions have been prepared via conventional solid state reaction route, while three different samples were prepared by mechano-chemical synthesis using ball-milling technique. The characterization of all the samples was done using XRD, complex impedance spectroscopy, modulus spectroscopy and dc conductivity investigation. All the impedance measurements have been carried out in the temperature range 200-675 $^{\circ}\text{C}$ with a sweep in frequency from 5Hz to 13 MHz. A regular variation for the conductivity as function of composition is observed for $\text{Li}_3\text{PO}_4\text{-x m/o Li}_2\text{S}$ system. The conductivities of all the samples lie in-between the conductivities of pure components Li_3PO_4 and Li_2S , which show minimum and maximum conductivity respectively. The conductivity enhancement results are supported by XRD patterns. An increase in the conductivity and a decrease in the activation energy is observed for 20,30 and 50 m/o Li_2S ball-milled samples compared to those of the conventionally prepared samples. The fact that the activation energy for the ionic conduction is same as that for the dielectric relaxation process, leads us to conclude that a single “conductivity” relaxation is the dominant mechanism.

Acknowledgement

I express a deep sense of gratitude to Professor K. Shahi for his consistent and invaluable guidance throughout the present thesis work. He has been constant source of inspiration with 'never give up' attitude. I am very much thankful to him for consistent encouragement throughout the research work.

I am grateful to all my labmates Anshuman, Jai Prakash, Sudha, Feroz, Manish and Anoop for their cooperation and encouragement throughout the present work.

I would like to thank all my friends-Ritesh, Ajay, Ambrish, Vibhor, Suneet who made my stay here full of love and warmness.

I express my sincere thanks to my classmates Neeraj, Abhishek, Animesh and Sreya for their support throughout my stay at IITK.

I am also thankful to Materials science & ACMS staff Mr.B.Sharma, Mr. Umashankar, Prasadji, Joshiji, Mr. Chaturi Singh, Mr. Kartikeyan, Pandeji and Physics workshop staff Mr. Sampati Singh and Omprakashji.

Contents

1 Introduction	1
1.1 Classification of Ionic Solids	1
1.1.1(a) Point Defect Type	1
1.1.1(b) Molten sublattice Type	1
1.1.2(a) Poor or Normal Ionic conductors	2
1.1.2(b) Moderate Ionic conductor	2
1.1.2(c) Fast Ionic conductors	2
1.1.3(a) Cationic conductors	3
1.1.3(b) Anionic conductors	3
1.2 Emerging Trends in Solid State Ionic conductors	4
1.2.1 Crystalline Ionic conductors	4
1.2.2 Amorphous Ionic conductors	4
1.2.3 Polymeric ionic conductors	4
1.2.4 Protonic conductors	4
1.2.5 Composite Ionic Conductors	5
1.3 Doping –An Aid to Enhance Conductivity	5
1.3.1 Homogeneous Doping	5
(i) Homovalent Doping	5
(ii) Aliovalent Doping	6
1.3.2 Heterogeneous Doping	6
1.4 General theory of Ionic Conductors	6

1.5 Dielectric Relaxation and Modulus spectroscopy	7
1.5 Maxwell Model for Composite Electrolytes	10
1.6 Present Investigation	11
2 Experimental Details and Characterization techniques	12
2.1 Experimental Set-Up Details	12
2.1.1 Sample Holder	12
2.1.2 Furnace and Temperature Controller	15
2.1.3 Impedance analyzer	15
2.2 Impedance Measurement	16
2.3 Materials Processing	17
2.4 Sample Preparation	17
2.5 Ball-Milling	18
2.6 Characterization Techniques	19
2.6.1 X-Ray Diffraction	19
2.6.2 Complex Impedance analysis	20
(i) Pure Resistor R	22
(ii) Pure Capacitor C	22
(iii) Series Combination of R and C	24
(iv) Parallel combination of R and C	24
2.7 Impedance Measurement Methodology	28

3 Results and discussion	30
3.1 Mechano-Chemical Synthesis using Ball milling technique	30
3.2 XRD	31
3.2.1 Conventional Samples	31
3.2.2 Ball-Milled Samples	36
3.3 Impedance analysis	40
3.3.1 Conventional Sample	40
3.3.2 Ball-Milled Samples	43
3.4 DC Conductivity	43
3.5 Composition vs. Conductivity	44
3.5.1 Conventional Sample	44
3.5.2 Ball-Milled Sample	48
3.6 Analysis of Dielectric Modulus	51
3.7 Activation Energy-A Comparison (Conventional Samples)	56
3.8 Effect of Milling on Activation energy	58
3.9 Activation Energy-A Comparison (Milled Samples)	59

Figure Caption

1.1	Modulus (M' , M'') vs. frequency plot	10
2.1	Block diagram of the experimental set-up used in the ionic conductivity measurement	13
2.2	Diagram of sample holder for impedance measurement	14
2.3	Impedance lot for a purely resistive circuit	23
2.4	Impedance plot for a purely capacitive circuit	23
2.5	Impedance plot for a resistor and a capacitor in series	24
2.6 (a)	Impedance plot for a resistor and a capacitor in parallel	26
2.6 (b)	Effect of interface capacitance C_i on impedance of electrolyte	26
2.6 (c)	Depression of semicircle	27
2.6 (d)	Grain boundary effect	27
3.1	XRD patterns for Li_3PO_4 , Li_2S and 5m/o Li_2S composition	33
3.2	XRD patterns for 10, 20m/o Li_2S composition	34
3.3	XRD patterns for 30, 50m/o Li_2S composition	35
3.4	XRD patterns for the 0, 73, 135 hours milled Samples of compositions 20 m/o	37
3.5	XRD patterns for the 0, 77, 188 hours milled Samples of compositions 30 m/o	38
3.6	XRD patterns for the 0, 27, 71 hours milled Samples of compositions 50 m/o	39

3.7 (a)	Impedance plot for Li_3PO_4 at 716, 752, 790 $^{\circ}\text{K}$	40
3.7 (b)	Impedance plot for Li_2S at 542, 588, 624 $^{\circ}\text{K}$	40
3.7 (c)	Impedance plot for 30m/o Li_2S composition at 537, 568 $^{\circ}\text{K}$	41
3.7 (d)	Impedance plot for 30m/o Li_2S composition at 602, 641 $^{\circ}\text{K}$	42
3.8	Impedance plot for Li_2S at 588 $^{\circ}\text{K}$	42
3.9 (a)	Impedance plot for 20m/o Li_2S composition (conventional) at 507, 536, 565 $^{\circ}\text{K}$	43
3.9 (b)	Impedance plot for 20m/o Li_2S composition (Milled) at 506, 531, 555 $^{\circ}\text{K}$	43
3.10	Log conductivity vs. inverse temperature plot Li_3PO_4 -xm/o Li_2S system	47
3.11	Log conductivity vs. inverse temperature plot for ordinary and milled (135 hours) samples of 20 m/o Li_2S composition	49
3.12	Log conductivity vs. inverse temperature plot for ordinary and milled (188 hours) samples of 30 m/o Li_2S composition	49
3.13	Log conductivity vs. inverse temperature plot for ordinary and milled (71 hours) samples of 50 m/o Li_2S composition	50
3.14 (a)	Modulus (M') spectra at 537 $^{\circ}\text{K}$ for 30m/o Li_2S Composition	51
3.14 (b)	Modulus (M') spectra at 568 $^{\circ}\text{K}$ for 30m/o Li_2S Composition	51
3.15 (a)	Modulus (M'') spectra at different temperatures for pure Li_3PO_4	52
3.15 (b)	Modulus (M'') spectra at different temperatures for 5m/o Li_2S composition	52

3.15 (c)	Modulus (M'') spectra at different temperatures for 30m/o Li_2S composition	53
3.15 (d)	Modulus (M'') spectra at different temperatures for 50m/o Li_2S composition	53
3.15 (e)	Modulus (M'') spectra at different temperatures for 70m/o Li_2S composition	53
3.15 (f)	Modulus (M'') spectra at different temperatures for pure Li_2S	53
3.16 (a)	M'/M'' dependence on frequency for 50m/o Li_2S Composition at 574 $^\circ\text{K}$	55
3.16(b)	M'/M'' dependence on frequency for 30m/o Li_2S Composition at 568 $^\circ\text{K}$	55
3.16 (c)	M'/M'' dependence on frequency for 30m/o Li_2S Composition at 537 $^\circ\text{K}$	55
3.17	Modulus (M'') spectra at different temperatures for 50m/o Li_2S (milled) composition	56

List of Tables

1.1	Conductivity of some ionic conductors	3
2.1	Displays of analyzer	16
2.2	The physical properties of starting materials	17
2.3	Sintering temperature, sintering time and thickness of samples prepared	18
2.4	Details of milling processing	19
3.1	Milling hours for different compositions	31
3.2	Observed and calculated values of conductivity For $\text{Li}_3\text{PO}_4\text{-xLi}_2\text{S}$ system at 713 $^{\circ}\text{K}$	46
3.3	Relaxation times for different compositions	54
3.4	Comparison of activation energies extracted from different processes for conventional samples	57
3.5	Activation energies before and after milling	58
3.6	Comparison of activation energies extracted from different processes for milled samples	59

Chapter 1

Introduction

The history of superionic conductors starts with Faraday's work on AgI in 1839^[1], but the work couldn't gain pace because of non-availability of good ionic conductors at moderate temperatures. The field of solid state Ionics achieved full rhythm in research after the discovery of fast sodium ion conduction in β -alumina, which has a sodium ion conductivity at room temperature comparable to that of an aqueous sodium chloride and silver ion conduction in MAg_4I_5 ($M=K, Rb, NH_4$) in 1967. Since then, a number of applications of different nature have been invented e.g. solid state batteries, fuel cells, sensors and memory devices.^[2]

Fundamental work on ionic conduction is carried out by many scientists from diverse fields. Frenkel and Schotteky proposed their classic mechanisms that explain how electricity can be conducted through ionic solids by the flow of ions. Frenkel disorder, in which ions move from normal lattice sites to interstitial sites and schotteky disorder by which volume of a crystal expands and vacancies are induced in normal lattice positions, gives a prompt picture of inside processes.^[3]

Basically the superionic conductor is the term used for the ionic conductors having ionic conductivity $\geq 10^{-3} \Omega^{-1} \text{cm}^{-1}$.

1.1 Classification of ionic solids

In ionic solids the presence of defects or disorder is a necessity to sustain significant ionic transport. They can be classified according to type of defects.

1.1.1(a) Point defect type

1.1.1(b) Molten sublattice type

In point defect type ionic solids transport is through thermally generated Frenkel and Schottky defect pairs. The activation energy is generally high $\sim 1\text{eV}$ or more for them. These point defect type solids can be further categorised according to defect concentration density:

(i) Dilute: The number of defects $\sim 10^{18}\text{ cm}^{-3}$ or less.

Examples are AgCl , $\beta\text{-AgI}$, NaCl , KCl etc.

(ii) Concentrated: The defect concentration $\sim 10^{20}\text{ cm}^{-3}$

Examples are Stabilized Zirconia or Hafnia, CaF_2 etc.

In molten sublattice type solids the number of sites available are more than the number of a particular type of ions. As a consequence all these ions hop or move like a free ion from one position to another. Since all these ions are available for transport, the conductivity is large and activation energy is low. These materials possess an average structure rather than the rigid structure.

In accordance to another classification scheme ionic solids can be divided into three groups based on their magnitude of conductivity at moderate temperatures.

1.1.2(a) Poor or Normal Ionic Conductors

The conventional ionic solids having an ionic conductivity $< 10^{-6}\ \Omega^{-1}\text{cm}^{-1}$ are placed in this group. The charge transport is through thermally generated Frenkel or Schottky defects.

Examples are alkali halides, AgCl , AgBr , $\beta\text{-AgI}$ etc.

1.1.2(b) Moderate Ionic Conductor

The range of conductivity for these ionic solids is from 10^{-6} to $<10^{-3}\ \Omega^{-1}\text{cm}^{-1}$.
Examples are CaF_2 , PbF_2 , CaO , ZrO_2 etc.

1.1.2(c) Fast ionic Conductors

In case of FIC, all the ions in a sublattice are available for movement, and conductivity is $>10^{-3}\ \Omega^{-1}\text{cm}^{-1}$. Examples are $\alpha\text{-AgI}$, RbAg_4I_5 , $\alpha\text{-Li}_2\text{SO}_4$.

In another way we can classify ionic solids as cationic and anionic conductors.

1.1.3(a) Cationic Conductors

- i) Li^+ and Na^+ ion conductors, e.g. LiI , Li_2SO_4 , $\text{Na-}\beta\text{-alumina}$, Na_3PO_4 ,
- ii) Cu^+ and Ag^+ ion conductors, e.g. $\alpha\text{-AgI}$, RbAg_4I_5 , $\alpha\text{-CuI}$,
- iii) Proton (H^+) Conductors e.g. H_3O^+ - β -alumina

1.1.3. (b) Anionic Conductors

- i) O^{2-} ion conductors, e.g. $\text{ZrO}_2+12\text{CaO}$, CeO_2+7SrO
- ii) F^- ion conductor, e.g. $\beta\text{-PbF}_2$, CaF_2 , SrF_2

Table 1.1: Conductivity of some Ionic conductors^[4]

Ionic Conductor	Conductivity ($\Omega^{-1}\text{cm}^{-1}$)	Temperature ($^{\circ}\text{C}$)
Li_3N	2.5×10^{-3}	27
LiAlCl_4	1.2×10^{-6}	27
CuTeBr	$\sim 10^{-5}$	25
RbCu_3Cl_4	2.0×10^{-3}	25
RbAg_4I_5	0.27	25
$\beta\text{-Ag}_3\text{SI}$	0.01	25
KbiF_4	1.7×10^{-4}	25
$\alpha\text{-PbSn}_4$	2.0×10^{-3}	25

1.2 Emerging Trends in Solid State Ionic Conductors.

1.2.1 Crystalline Ionic Conductors

The structure and composition of ionic solids are optimized for high ionic conductivity, the mechanisms by which the ions diffuse rapidly in these materials are related to those that lead to ionic conductivity in classical ionic solids such as NaCl, BaCl₂ and LiI. Examples are Na-- β alumina, NASICON, Stabilized ZrO₂, RbAg₄I₅ etc.^[5]

1.2.2 Amorphous Ionic Conductors

All the ions to be potentially conducting but in a broad distribution of state, lack of grain boundaries, isotropic and generally higher conductivities are the distinct advantages of amorphous (glassy) ionic conductors over their crystalline counterparts. Examples are alkali germanate glasses.^[6,7]

1.2.3 Polymeric Ionic conductors

Solid polymer electrolytes attracted considerable attraction since their discovery by Armand, because they possesses many advantages over inorganic solid electrolytes, for example easy to make film, has good elasticity and deformability during charge and discharge in an all-solid secondary batteries. Polymer electrolytes based on Lithium salts (LiX) and PEO were extensively studied in recent years, but its ambient conductivity is too low. The reason for such a low conductivity is the presence of crystalline part in PEO. The cross-linking is an effective method to enhance conductivity of PEO.

1.2.4 Protonic Conductors

Proton conducting solids have been widely investigated in a view of their application in many electrochemical devices like fuel cells, batteries, sensors, display devices etc. The phosphotungstic acid (H₃PW₁₂O₄₀.nH₂O: PTA) and

phosphomolybdic acid ($\text{H}_3\text{PMO}_{12}\text{O}_{40} \cdot n\text{H}_2\text{O}$: PMA) are good proton (H^+) conductors. The room temperature conductivity could be as high as 10^{-1} - $10^{-2} \Omega^{-1}\text{cm}^{-1}$ at very high humidity levels and varies strongly with humidity as number of water molecules (n) varies with it.^[8]

1.2.5 Composite Ion Conductors

The doping with an insulator material or other ionic conductors may lead to the enhancement in the conductivity of matrix ionic conductor. Jow and Wagner proposed that the dispersion of the insulating particles in the host matrix produces a space charge layer at the matrix/particle interface, and thus facilitates the ionic motion. The dispersion of SiO_2 in AgI leads to conductivity enhancement in AgI- SiO_2 system.^[9]

1.3 Doping – An aid to enhance conductivity

In composite solid electrolytes conductivity can be enhanced by doping. It can be done in two ways:

1.3.1 Homogeneous Doping

In order to improve the ionic conductivity of normal ionic conductor, defect concentration has been influenced by adding an appropriate material to the host matrix. It can be further classified in two types:

(i) Homovalent doping

Substitution of the ions having the same valency but different size influences the ionic conductivity of the host material. Investigations on mixed crystals have revealed that the effect of built-in wrong size of the homovalent ion depends strongly on the size difference of between the host and the guest ion.^[10]

The lattice-loosening model says that the substitution of a monovalent ion having size different than host ion introduces a strain in the lattice, which ultimately leads to an increase in the conductivity.

(ii)Aliovalent doping

When host ion system is doped with an ion of different valency, excess defects are created to fulfill the charge neutrality need. The doping of alkali halides (MX) with divalent cations. ($M'X$, where $M' = \text{Ca, Mg etc.}$) or anions (S^{2-}, CO_3^{2-}) is a good example of aliovalent doping

1.3.2 Heterogeneous Doping

The overall conductivity of a two-phase mixture may exceed the conductivity value of pure constituents. In one case Li^+ ion conductivity enhancement takes place in LiI containing fine Al_2O_3 particles, while AgI-AgBr is another example.

1.4 General Theory of Ionic Conductors

The electrical conductivity of any material is given by,

$$\sigma = \sum_i n_i q_i \mu_i \quad (1.1)$$

Where n_i , q_i , μ_i are the concentration, the charge, and the mobility respectively of the 'i' th species. In ionic solids ions are dominating conductivity species. So the Eq. 1.1 becomes,

$$\sigma = nq\mu \quad (1.2)$$

Where $q = ze$ (z is the valency of the mobile ion and e is the electronic charge).

Thermally induced interstitial ions (Frenkel defects) or vacancies (shottky defects) are basically are the charge carriers responsible for conduction in moderate ionic conductors. The equilibrium concentration of either type of defects is given to a good approximation by:

$$n = Bn_0 \exp\left[\frac{-G_f}{2kT}\right] \quad (1.3)$$

Where G_f is the free energy of formation of a defect pair at the temperature T , n_0 is the concentration of the normal lattice sites, and B is an entropy factor, which depends on the crystal structure, and the type of defect involved.

$$\mu = A \frac{a^2 e \nu}{kT} \exp \left[\frac{-G_m}{kT} \right] \quad (1.4)$$

Where G_m is the free energy of migration of the mobile species through the lattice, ν is the frequency of vibration, a the jump distance, and A is a factor which accounts for the change in G_m with temperature.

A general expression for conductivity (σ) can be obtained on combining the Eq. 1.2, 1.3, and 1.4

$$\sigma = \frac{C}{T} \exp \{ \{-G_f / 2\} - (G_m) / kT \} \} \quad (1.5)$$

In terms of the corresponding enthalpy (H) and entropy (S),

$$G_f = H_f - TS_f \quad (1.6)$$

$$G_m = H_m - TS_m \quad (1.7)$$

Eq.(1.5) can be rewritten as:

$$\sigma = (\sigma_0 / T) \exp \{ \{(-H_f / 2) - H_m\} / kT \} \} \quad (1.8)$$

$$\text{or, } \sigma T = \sigma_0 \exp [-E_a' / kT] \quad (1.9)$$

Where $E_a' = ((H_f / 2) + H_m)$ is the overall activation energy for conduction. Thus a plot of $\log(\sigma T)$ vs. $1/T$ is linear whose slope yields the overall activation energy

$$E_a' = ((H_f / 2) + H_m). \quad (1.10)$$

Generally a plot of $\log \sigma$ versus $1/T$ for a pure ionic solid consists of two linear segments: a high temperature linear region, which is an intrinsic property of the material, and a low temperature extrinsic region characterized by a lower slope.

1.5 Dielectric Relaxation & Modulus spectroscopy

By definition dielectric constant can be written as,

$$\varepsilon^* = \frac{Y^*}{j\omega C_0} \quad (1.11)$$

Where ε^* is the dielectric constant, ω is the frequency of applied signal and C_0 is the air capacitance and Y^* is the complex admittance. Eq.(1.11) can be rewritten as:

$$\varepsilon' - j\varepsilon'' = \frac{1}{Z^* \omega C_0} \quad (1.12)$$

$$= \frac{1}{(Z' - jZ'')j\omega C_0} \quad (1.13)$$

$$= \frac{(Z' + jZ'')}{(Z'^2 + Z''^2)} \quad (1.14)$$

$$= \frac{Z' + jZ''}{Z^2 j\omega C_0} \quad (1.15)$$

Comparing the real and imaginary parts on both sides:

$$\varepsilon' = \frac{Z''}{Z^2 \omega C_0} \quad (1.16)$$

$$= \frac{\sin \theta}{Z \omega C_0} \quad (1.17)$$

$$\varepsilon'' = \frac{Z'}{Z^2 \omega C_0} \quad (1.18)$$

$$= \frac{\cos \theta}{Z \omega C_0} \quad (1.19)$$

The Complex Modulus, which is reciprocal of complex dielectric constant is given by:

$$M^* = \frac{1}{\epsilon^*} \quad (1.20)$$

$$= Z^* j\omega C_0 \quad (1.22)$$

$$\text{or } M' + jM'' = (Z' - jZ'')j\omega C_0 \quad (1.23)$$

$$M' = Z'' \omega C_0 \quad (1.24)$$

$$= Z \sin \theta \omega C_0 \quad (1.25)$$

and

$$M'' = Z' \omega C_0 \quad (1.26)$$

$$= Z \cos \theta \omega C_0$$

Modulus spectroscopy is a popular tool to investigate study of electrochemical system.^[11]

Under an ac field dispersion or dielectric relaxation is observed due to a number of different polarization mechanisms. The presence of any dielectric relaxation that corresponds to one or more of the possible polarization mechanisms that occur on a microscopic scale. Each relaxation process may be characterized by a relaxation time, which describes the decay of its polarization with time in a periodic field.^[12]

The plot between M' or M'' and $\log\left(\frac{\omega}{2\pi}\right)$ is called modulus spectra. The ideal modulus spectra plots are shown in Fig. 1.1.

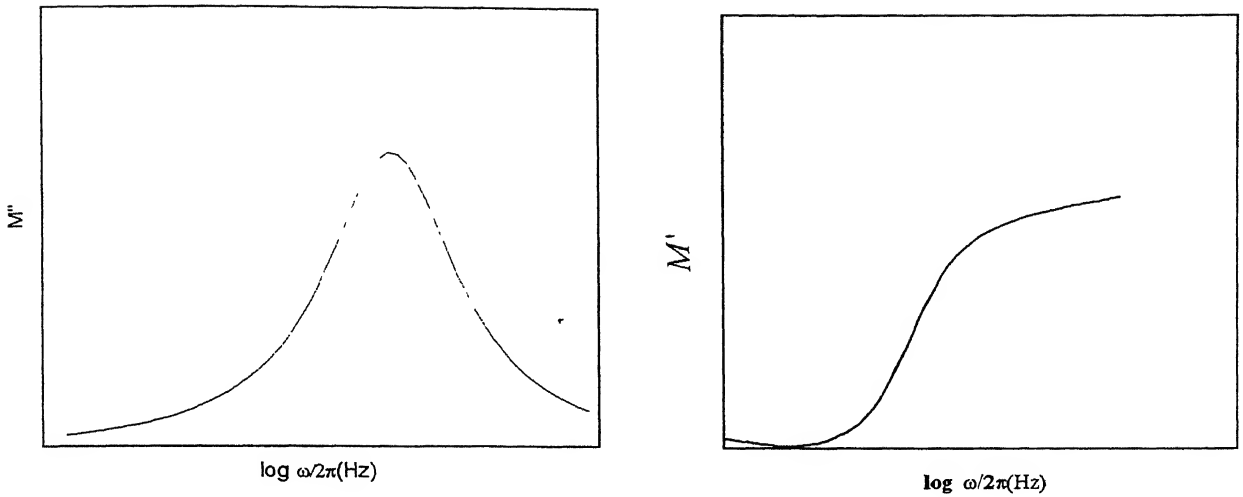


Fig. 1.1: Modulus(M' , M'') vs. frequency plots

1.6 Maxwell Model for Composite Electrolytes

In the classical theory proposed by Maxwell the conductivity of a two-phase mechanical mixture has been calculated in terms of the bulk conductivities of the individual phases.

A composite electrolyte is having two constituents with mole fraction f_1 and f_2 . Let the conductivities of the first and second electrolyte are σ_1 and σ_2 respectively. Then according to Maxwell's classical theory conductivity of the composite electrolyte can be given by:

$$\sigma_{\text{composite}} = f_1\sigma_1 + f_2\sigma_2 \quad (1.26)$$

Therefore conductivity of any m/o composition will always lie in-between the bulk conductivities of the pure constituents. An enhancement in conductivity will occur as molar fraction of the higher conducting solid increases.^[13]

1.7 Present Investigation

The electrical conductivity of solid electrolyte is an important parameter, which influences the range and types of their application. Fast Lithium ion conductors have attracted much interest in recent years in view of development of high energy density batteries. The ionic mass of lithium makes it a promising material for such applications. As the Li_3PO_4 was the starting material, which is having good ionic conductivity at high temperatures, with a view to get a better ionic conductor it was doped with Li_2S , which is a favorable material for fast ionic conduction. To record and observe the conductivity results and to perform dielectric studies on the resulting compositions was the aim behind the work. The mechano-chemical synthesis using milling technique has also employed to get better and stable superionic conductor.

Chapter2

Experimental Details and Characterization Techniques

2.1 Experimental Set-Up Details

The diagram 2.1 gives an idea of the experimental set-up for impedance measurement. The material whose conductivity studies, dielectric studies has to be performed is palletized in cylindrical form and is placed between two silver discs of diameter 11mm. silver wires are brazed (using gas welding) to silver disc to provide connection to impedance analyzer, the chromel –alumel thermocouple is used to measure the temperature of the sample. A special type of sample holder was fabricated to place the pellet along with the thermocouple, inside the furnace. A temperature controller (Indothrem 401D) was used to control the furnace temperature. A Kiethly (Model: Autoranging Microvolt DMM) digital multimeter was used to record the thermocouple voltage in millivolts. The various instruments and equipment used in the set-up are individually discussed ahead.

2.1.1 Sample Holder

A special type of sample holder (Indigenously designed by Solid State Ionics Lab) was fabricated for impedance measurement. Fig. 2.2 shows the schematic diagram

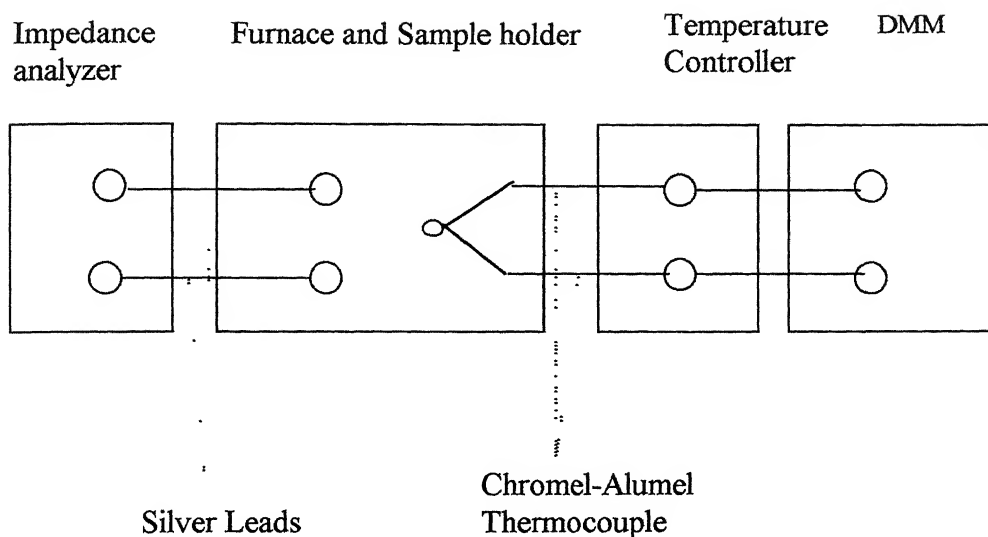


Fig. 2.1: Block diagram of the experimental set-up used in the ionic conductivity measurements

of the sample holder. It consists of three identical lava discs (diameter=2.5 cm, thickness=1.1 cm) and a Bakelite block (diameter=2.5 cm, thickness=5 cm), each having a hole at center and other four holes are symmetrically located along the periphery. There is a cylindrical grove of depth 0.1 cm and diameter 1.2 cm on lava disc in order to fit quartz tube and spring. The lava discs after machining was heated slowly to 700 °C and kept at that temperature for five hours to harden them. A pair of stainless steel rods was passed through the two diametrically opposite holes to provide support to the sample holder.(Fig. 2.2)

The spring is in between lava disc and Bakelite block & this portion of the sample holder is out of the furnace. There is a 20mm long quartz tube (dia 1.1 cm) in between two lava discs .The spring and quartz tube are for the purpose of providing proper pressure between silver electrodes & sample to give a good

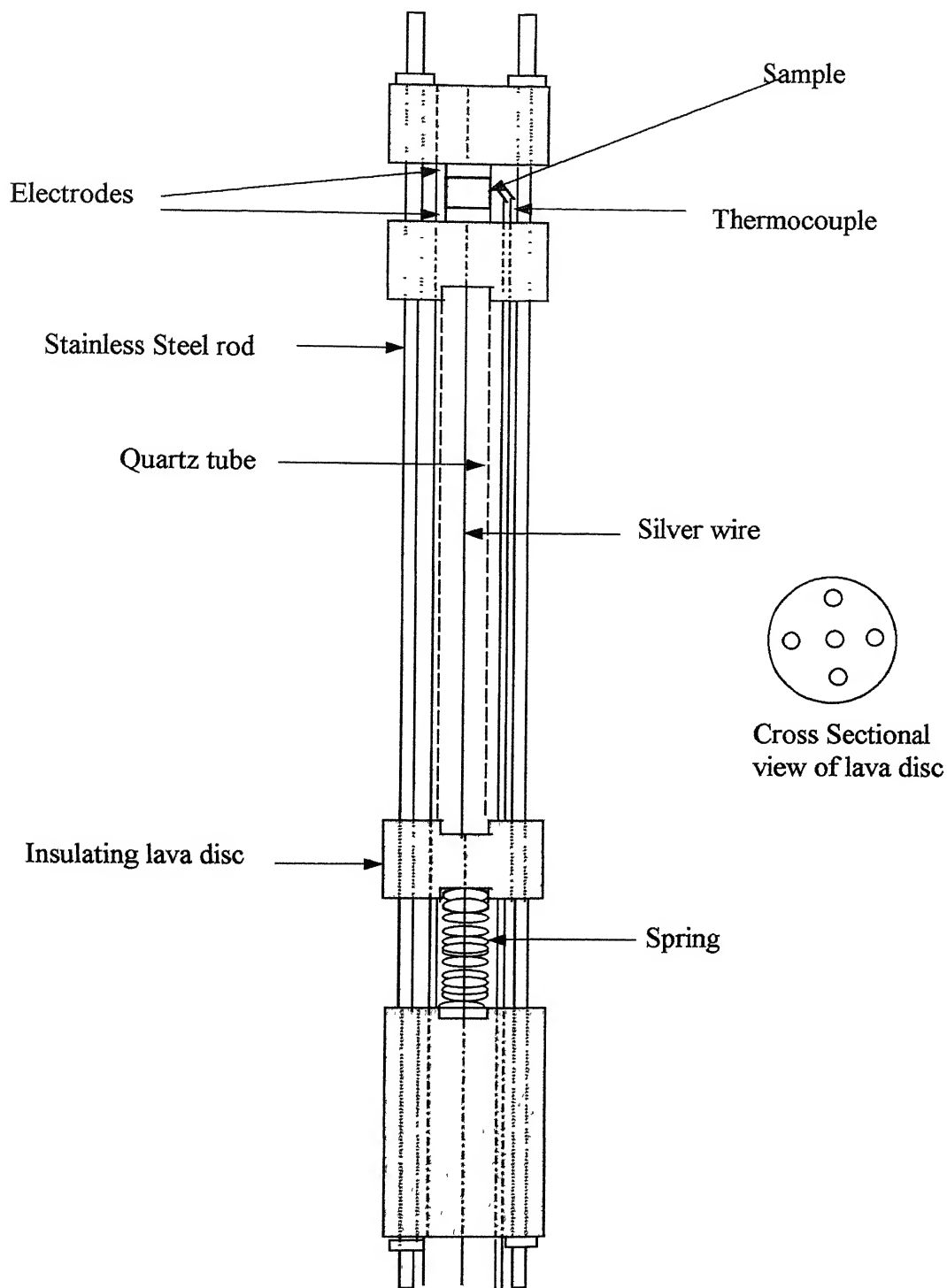


Fig. 2.2: Diagram of sample holder for Impedance Measurement

Contact among them. The silver wires are brazed to silver electrodes using brass to provide a high temperature bearing capacity to electrode wire joint. The sample holder also holds a chromel-alumel thermocouple, which senses the temperature of the sample.

2.1.2 Furnace and temperature controller

An electrical resistance heating furnace comprising of a mullite tube (Internal diameter ~ 4.9 cm), over which kanthol wire was wound uniformly, has been used. The resistance of the heating element was 28.2Ω . A high temperature cement was applied over the kanthal winding to fix it at place. The mullite tube with cemented kanthal wiring was enveloped with a cylindrical stainless steel container and the space between mullite tube and steel container was filled with glass wool in order to minimize the heat loss.

A chromel-alumel thermocouple was employed to measure the temperature of the sample. A DMM is connected to output of this thermocouple and moreover a PID type temperature controller (Indotherm 401D) has been used to control the temperature of the furnace. The output of the thermocouple is fed to temperature controller, which compares set temp. & actual temp. and accordingly supplies the required power to the furnace. The accuracy of the DMM used is $1\mu V$.

2.1.3 Impedance Analyzer

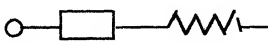
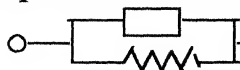
A HP 4192A fully automatic impedance analyzer along with a HP 1607A-test fixture is employed for wide range of complex impedance measurement. The instrument has an auto balancing bridge with a test signal from 5mV to 1mV. The built in frequency synthesizer can be set to measuring frequency within the range from 5Hz to 13MHz with 1mHz minimum resolution. The two display modes 'A' or 'B' can be selected to measure the quantities of interest.

2.2 Impedance Measurement

HP 4192A impedance analyzer was used to measure the impedance Z and the phase angle θ . The frequency was swept from 5Hz to 13MHz for each temperature. For dielectric measurements the displays can be set to 'C' and 'D' to obtain ϵ' and ϵ'' , but the dielectric quantities are possible to be calculated with only Z and θ values.

Table 2.1: The Displays 'A' and 'B' of Impedance Analyzer

Display A Function	Display B Function
$ Z $: Absolute value of Impedance	$\theta(\text{deg/rad})$:Phase Angle
$ Y $: Absolute value of Admittance	
R : Resistance	X : Reactance
G : Conductance	B : Susceptance
L : Inductance C : Capacitance	Q : Quality Factor
	D : Dissipation Factor
	R : Resistance
	G : Conductance

The equivalent circuit modes are auto,  (Series), and  (Parallel).

2.3 Materials Processing

Starting materials were Li_3PO_4 and Li_2S

Table 2.2 The Physical Properties of the Starting Materials

	Li_3PO_4	Li_2S
Supplier	Alfa Products, USA	Alfa Products, USA
Purity	99+%	99+%
Molecular Weight	115.79	45.94
Density(gm/cc)	2.537	1.66

2.4 Sample Preparation

The starting materials Li_3PO_4 and Li_2S were kept inside a dry box containing P_2O_5 to absorb any moisture present inside the dry box. Mixed crystals of different compositions were prepared by weighing appropriate amounts of Li_3PO_4 and Li_2S using electronic balance. Then the mixture was transferred to agate mortar and ground well to make a homogenized mixture. A special steel die (Fig.) of inner dia 11mm was used to make pellets. The mixture has been transferred to the die and die has been placed in a punch and a pressure of 4.4 ton has been employed to make pellets. The pellets of dia 11mm are now placed in an alumina crucible, which is placed inside the furnace for the purpose of sintering at appropriate temperatures for 5 hours. Now graphite paint has been applied to the two flat surfaces of the sintered pellets and dried in an oven at around 120°C . The pellet is loaded to the sample holder with chromel alumel thermocouple to measure the temperature of the sample. Now measurements are carried out using 4192A Impedance analyzer

Table 2.3: Sintering temperature, sintering time and thickness of different samples prepared. (Pelletization Pressure 4.4 ton/cm²)

Composition	Sintering temperature	Time	Thickness of the Pellet(cm)
Li ₃ PO ₄ (Pure)	790 °C	5hrs	0.392
Li ₃ PO ₄ + 5m/oLi ₂ S	790 °C	5hrs	0.304
Li ₃ PO ₄ + 10m/oLi ₂ S	790 °C	5hrs	0.260
Li ₃ PO ₄ + 20m/oLi ₂ S	790 °C	5hrs	0.290
Li ₃ PO ₄ + 30m/oLi ₂ S	790 °C	5hrs	0.260
Li ₃ PO ₄ + 50m/oLi ₂ S	790 °C	5hrs	0.306
Li ₃ PO ₄ + 70m/oLi ₂ S	790 °C	5hrs	0.232
Li ₂ S(Pure)	450 °C	5hrs	0.170

2.5 Milling

Crystalline raw materials of Li₃PO₄, Li₂S were used as starting materials. The materials are mixed in the appropriate mole ratio in an agate mortar beforehand. The mechanical milling treatment was carried out on the mixture using a Fritsch (Germany) Planetary Ball Mill at room temperature. Agate pots and balls were used for milling process. Acetone has been added to the mixture in a fixed amount at fixed time to get a homogeneously milled sample.

The sample material in the planetary ball mill is primarily crushed by the high-energy impact of grinding balls and in part by friction between the balls and the wall of the grinding bowl. The grinding bowls with material and balls rotate around their own axis on a counter-rotating planetary disc. The centrifugal forces caused by the rotation of the grinding bowls and supporting discs work on the contents of the grinding bowls. The force resulting from rotation of the grinding bowl when the mill is started causes the rotating balls to rub against the inside wall of the bowl thus crushing the material at a certain point in time the stronger

centrifugal force of the planetary disc causes the grinding material and balls to separate from the inner wall of the grinding bowl. the grinding balls cross the bowl at high speeds impacting with the grinding material on the opposite wall-creating size reduction by impact.

The different parameters for milling are summarized below:

Table 2.4 : Details of Ball-Milling Processing

- Fritsch(Germany)Planetary Ball mill .
- Agate pot and balls
- Volume of pot=250cc
- Weight of starting material=2.0 gms.
- Diameter of agate balls=6mm
- Ball mill speed=600rpm

After milling powered sample has been pelletized using Press. These pellets (prepared from milled material) are not sintered and after applying graphite paint mounted directly to the sample holder for the measurements.

2.6 Characterization Techniques

2.6.1 X-ray diffraction

X-ray diffraction of various compositions has been recorded using a computerized Richeifert(ISO-debyeflex 2002) power diffractometer employing a filtered CuK_{α} radiation ($\lambda=1.542 \text{ \AA}$). The generator was operated at 30KV and 30mA. The generator scanning speed was 3° per minute in 2θ . All XRD patterns were recorded at room temperature.

2.6.2 Complex Impedance Analysis

The Concept

In impedance spectroscopy various physical processes occurring in electrolyte/electrodes can be modeled as a combination of resistance and capacitances. After Bauerle's classic paper the ac impedance spectroscopy has found rapidly increasing favor as a tool for investigating solid electrolytes, electrode materials and the interfacial regions between them. In order to extract dc resistance, ac signal is applied to measure impedance so as to avoid the effect of polarization at electrode/electrolyte interface. A researcher Boukamp developed a package for for impedance/admittance analysis^[14,15]

The most common approach is to measure impedance directly in the frequency domain by applying a single frequency voltage to the solid electrolyte & measuring the phase shift and amplitude, using an impedance analyzer.

An ac sinusoidal signal $v(t) = V_M \sin(\omega t)$, involving the single frequency $\nu = \omega / 2\pi$, is applied to a cell and the steady state current $i(t) = I_M \sin(\omega t + \theta)$ is measured. Here θ is the phase difference between voltage and current.

Complex Impedance, $Z^*(\omega) = v(t)/i(t)$

Magnitude, $Z(\omega) = V_M / I_M(\omega)$

Phase angle $= \theta(\omega)$

The Complex impedance $Z^*(\omega)$ at an applied frequency can be written as: (2.1)

$$Z^*(\omega) = Z'(\omega) + jZ''(\omega)$$

Where Z' is the real and Z'' is the imaginary part of the complex impedance, which can also be represented as, (2.2)

$$Z' = Z \cos \theta \quad \& \quad Z'' = Z \sin \theta$$

Therefore magnitude of the complex impedance is, (2.3)

$$Z = (Z'^2 + Z''^2)^{1/2}$$

and the phase angle is,

$$\theta = \tan^{-1}(Z'' / Z')$$
 (2.4)

The impedance obtained is the combination of solid electrolyte, electrodes and electrical lead impedances. Physical properties can be modeled with the combination of resistors and capacitors, in order to analyze them. Therefore one can define that complex impedance analysis (CIA) is nothing but the measurement of impedance as a function of frequency. After measuring impedance for various frequencies, the real part Z' vs. imaginary part Z'' can be plotted. If the plot gives the rise to a semicircle then the diameter of the semicircle is nothing but the dc resistance that is independent of the frequency. Therefore CIA is highly useful in retrieving the dc conductivity of the sample.

(i)Pure Resistor R

For a pure resistor , complex impedance can be written as:

(2.4)

$$Z^* = R$$

Therefore real part of complex impedance,

(2.5)

$$Z' = R$$

and the imaginary part is,

(2.6)

$$Z'' = 0$$

\Rightarrow Impedance is frequency independent in this case. Therefore in impedance plot we will get a point only as shown in Fig.2.3

(ii)Pure Capacitor C

For a pure capacitor,

(2.7)

$$Z^* = \frac{1}{j\omega C}$$

$$= -\frac{j}{\omega C}$$

(2.8)

On comparing with eq. 2.1

$$Z' = 0$$

(2.9)

$$Z'' = -\frac{1}{\omega C}$$

Corresponding plot will give a straight line parallel to Z'' axis at $Z' = 0$ as shown in Fig. 2.4.

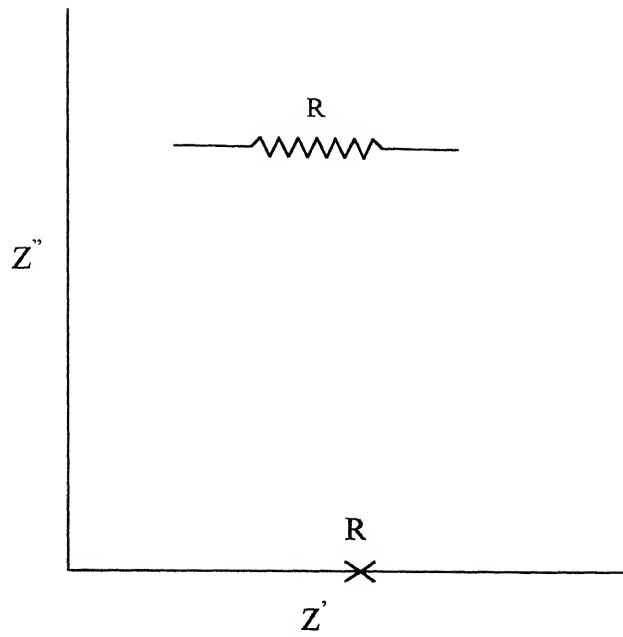


Fig. 2.3: Impedance plot for a purely resistive circuit

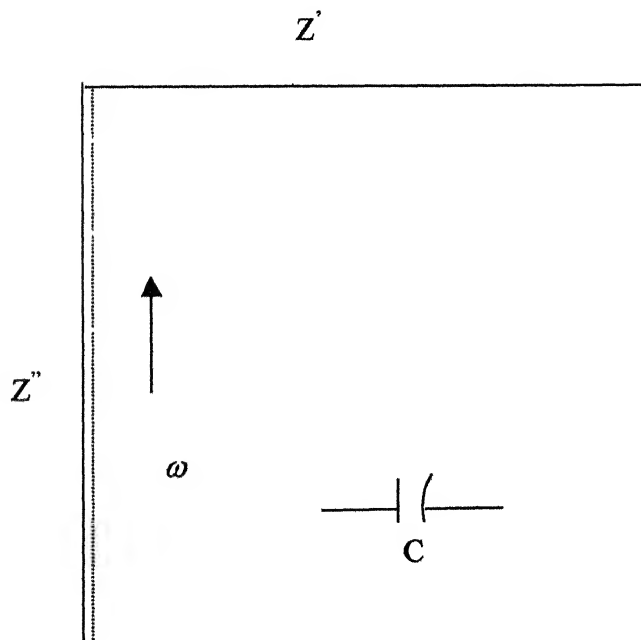


Fig. 2.4: Impedance plot for a purely capacitive circuit

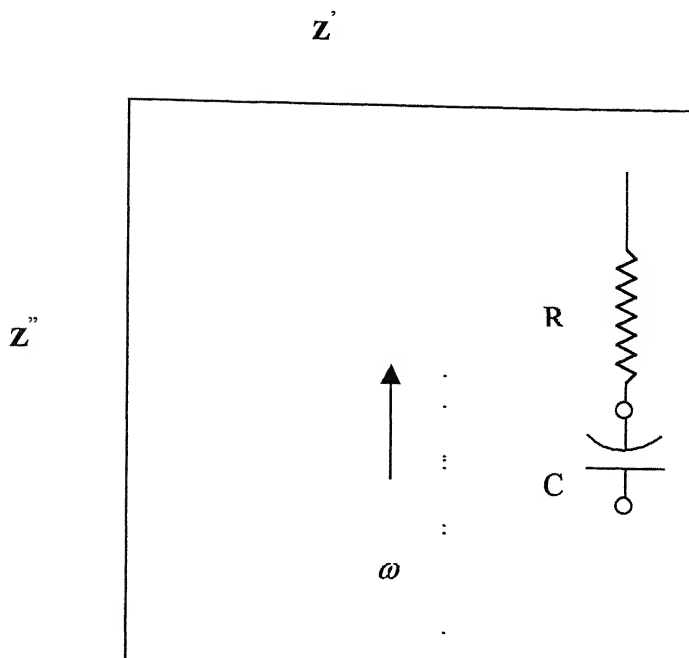


Fig. 2.5: Impedance plot for a resistor and a capacitor in series

(iii) Series Combination of R and C

For a series combination of R and C,

$$Z^* = R + \frac{1}{j\omega C} \quad (2.10)$$

$$= R + j\left(-\frac{1}{\omega C}\right) \quad (2.11)$$

Comparing with eq. 2.1

$$Z' = R, \quad Z'' = -\frac{1}{\omega C} \quad (2.12)$$

This combination will lead to a straight line parallel to Z'' axis with $Z' = R$

iv) Parallel Combination of R and C

Complex impedance for this system can be given as,

$$Z^* = \frac{R \left(\frac{1}{j\omega C} \right)}{R + \frac{1}{j\omega C}} \quad (2.13)$$

$$\text{or} \quad Z^* = \frac{R}{1 + \omega^2 C^2 R^2} + j \left(-\frac{\omega C R^2}{1 + \omega^2 C^2 R^2} \right) \quad (2.14)$$

Thus the real and imaginary parts can be given as.

$$Z' = \frac{R}{1 + \omega^2 C^2 R^2} \quad (2.15)$$

$$Z'' = -\frac{\omega C R^2}{1 + \omega^2 C^2 R^2} \quad (2.16)$$

Eliminating ω from these two equations,

$$Z'^2 + Z''^2 = R Z' \quad (2.17)$$

$$\text{or} \quad (Z' - R/2)^2 + Z''^2 = (R/2)^2 \quad (2.18)$$

Which is nothing but the equation of a circle with radius $R/2$ and centre at $(R/2, 0)$.

The diameter of the circle = R , which is the dc resistance of the sample.

Fig. 2.6(a) shows impedance plot when non-blocking electrodes are used. When blocking electrodes are used, an electrode/electrolyte interface capacitance C also comes into picture. This additional capacitance gives rise to a straight line at 90° for perfectly smooth surface. The slope of line decreases as the surface roughness increases as in Fig. 2.6(b)

Some polycrystalline materials show depression of semicircle in impedance plot. More specifically the lowering of the center of the high frequency impedance semicircle below the real axis takes place. This can be modeled as a constant phase element (CPE) in parallel with a resistance R as shown in Fig. 2.6(c). The admittance of the CPE can be represented by,^[16-19]

$$Y_{CPE}^* = A(\omega)^\alpha \quad (2.19)$$

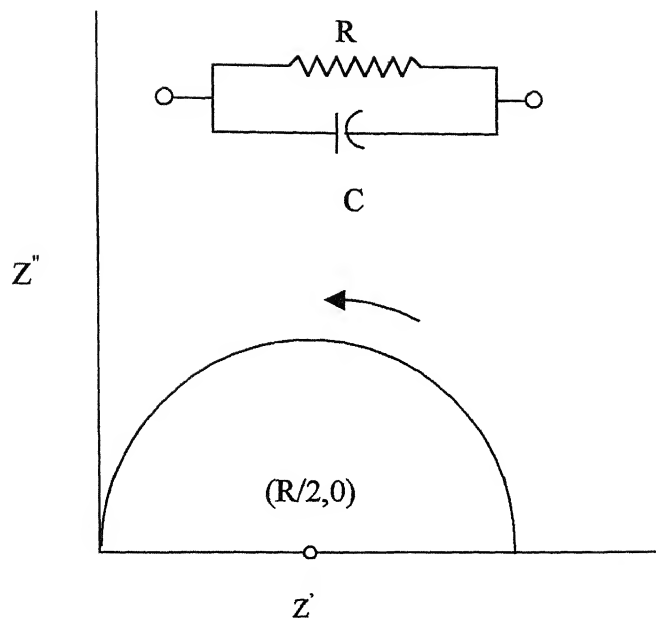


Fig. 2.6(a): Impedance plot for a resistor and a capacitor in parallel

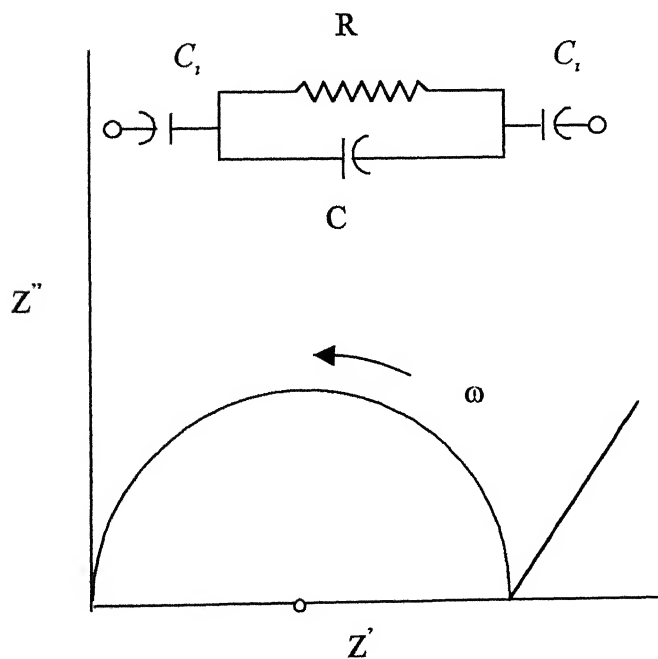


Fig. 2.6 (b): Effect of interface capacitance C_i on impedance of electrolyte

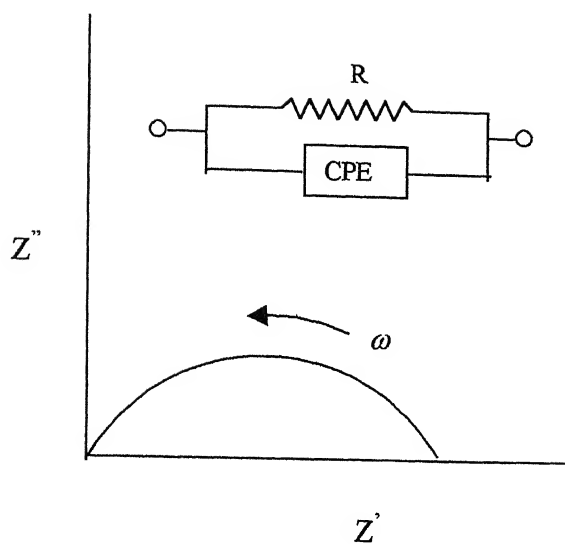


Fig. 2.6(c): Depression of Semicircle

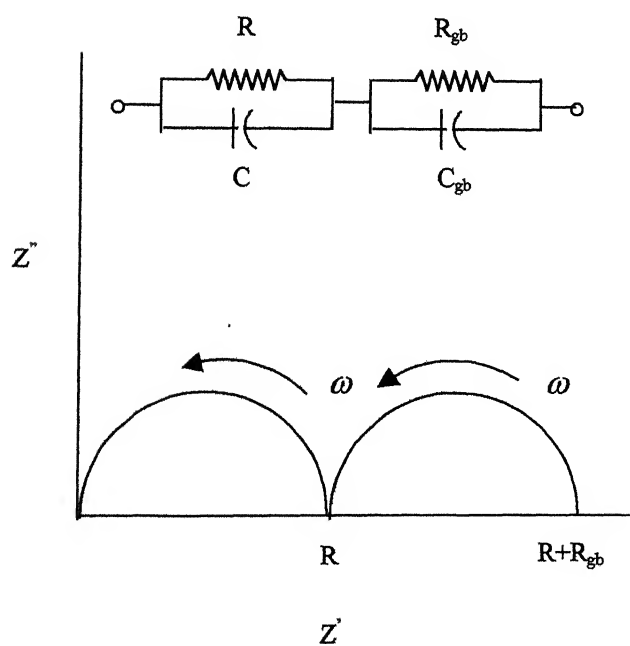


Fig. 2.6(d): Grain boundary effect

In poly-crystalline materials, close to grain boundaries, the transport properties of a crystal are controlled by imperfections expected to be present there in higher concentration than in the center of a grain, leading to an additional contribution to the inter-grain impedance which is exhibited two semicircles in the impedance plot of Fig. 2.7(d). R is the resistance of the bulk and R_{gb} is the grain boundary resistance. The diameter of the higher frequency semi-circle gives the dc resistance of the bulk.

The simplicity of the method is a prime advantage of impedance spectroscopy. The materials can be characterized by analysis of its observed impedance response leading to estimates of its microscopic parameters such as charge mobilities, concentrations etc. The disadvantage of the method is associated with possible ambiguities in interpretation.

2.7 Impedance Measurement Methodology

All the impedance measurements for different compositions were carried out using HP4192A impedance analyzer. The sample is loaded to the sample holder & placed in the furnace. Now spot frequency (f) was swept from 5Hz to 13MHz for a particular temperature and values of f , Z , θ , C , D has been noted down. Impedance plots (Z' vs. Z'') have been drawn during the experiment itself using MATLAB to ensure that proper points are available. The dc resistance (R_{dc}) has been observed wherever impedance plots are coming in semicircular fashion. The diameter of the semicircle has been considered as R_{dc} . This R_{dc} has been used to find dc conductivity (σ_{dc}) using the equation as below:

$$\sigma^* = \frac{l}{R_{dc} A} \quad (2.20)$$

Wherever impedance plot is not coming in semicircular fashion, $\frac{Z}{\cos \theta}$ at 10kHz

has been used as R_{dc} . this can be further explained as;

The conductivity can be given as,

$$\sigma^* = \frac{l}{Z^* A} \quad (2.21)$$

$$= \frac{l}{(Z' + jZ'')A} \quad (2.22)$$

$$= \frac{l}{(Z'^2 + Z''^2)A} (Z' - jZ'') \quad (2.23)$$

Therefore the real part of the conductivity (σ' or σ_{dc}) can be given as;

$$\sigma_{dc} = \frac{l}{(Z'^2 + Z''^2)A} Z' \quad (2.24)$$

$$= \frac{l}{(Z^2)A} Z' \quad (2.25)$$

$$= \frac{l}{Z^2 A} Z \cos \theta \quad (2.26)$$

$$= \frac{l \cos \theta}{ZA} \quad (2.27)$$

$$= \frac{l}{Z / \cos \theta \cdot A} \quad (2.28)$$

Therefore $Z / \cos \theta$ can be used in place of R_{dc} .

Enough time is provided between two readings to ensure the stability & accuracy of the results thereafter. All the experiments have been repeated twice to ensure reproducibility of results.

Chapter 3

Results & Discussion

In search of a new composite Li^+ superionic conductor based on Li_3PO_4 and Li_2S , samples of 0,5,10,20,30,50,70,100 m/o Li_2S - Li_3PO_4 were prepared via conventional solid state reaction route. However a few samples of 20,30 and 50 m/o Li_2S composition have also been prepared by mechano-chemical synthesis using ball-milling technique. Impedance measurements have been carried out for all the samples with a sweep in frequency from 5Hz to 13MHz. The dc conductivity, XRD, and modulus spectroscopy (relaxation phenomenon) results are discussed below.

3.1 Mechano-Chemical synthesis using ball milling Technique:

In order to produce better and stable superionic conductors ball-milling technique has been employed. This mechano-chemical process may sometimes lead to amorphisation of the crystalline constituents as seen in some silver-based systems.^[20]

With an aim to get better conductivity and stability, three compositions viz. 20, 30 and 50 m/o Li_2S were ball-milled one by one. The XRD patterns for starting crystalline compositions have been recorded. The parameters set for this process are discussed earlier in section 2.5. The acetone was added to the mixture after an interval of 4-5 hours of milling. The XRD patterns have been recorded after every

10-15 hours of milling to see the effect of milling on the system. The number of hours of milling for different compositions have been given in Table 3.1 . The results for all three milled compositions are summarized as under:

Table 3.1: Milling duration for different compositions

Composition (m/o Li_2S)	Duration of milling (hours)
20	135
30	188
50	71

3.2 XRD

3.2.1 Conventional Samples

The x-ray diffraction patterns give information about the constituent phases present in the test sample and the formation of compound, if any, as a result of reaction between the constituents. The XRD patterns for 0, 5, 10, 20, 30, 50, 100m/o Li_2S compositions have been recorded using computerized Richeifert (ISO-debyeflex 2002) powder diffractometer. All the XRD patterns are recorded at room temperature and some of these results are shown in Figs. 3.1-3.3.

No characteristics peaks of Li_2S (major peak at $2\theta = 28.5, 29.5$: double peak) are visible in the 5 and 10m/o Li_2S samples while all the characteristic peaks of Li_3PO_4 are visible. Therefore it may be inferred from these XRD patterns that the complete or partial solid solution has been formed.

For 20m/o Li_2S composition some of XRD peaks have grown longer in comparison to these for 5 and 10 m/o Li_2S compositions. Assuming that

PO_4^{3-} ion is being substituted by S^{2-} ion and that S^{2-} ion is smaller, the peak height should actually decrease. From these results it is thus concluded that either partial solid solution or a two-phase mixture is formed. For 30m/o Li_2S sample a double peak (at 2θ slightly less than 30°) is visible signifying that this sample is certainly a two-phase mixture. Similarly for 50m/o Li_2S composition the said double peak corresponding to Li_2S is clearly visible in addition to all the major peaks of Li_3PO_4 . It is thus concluded that Li_3PO_4 - Li_2S is a two-phase composite material over most of the composition range.

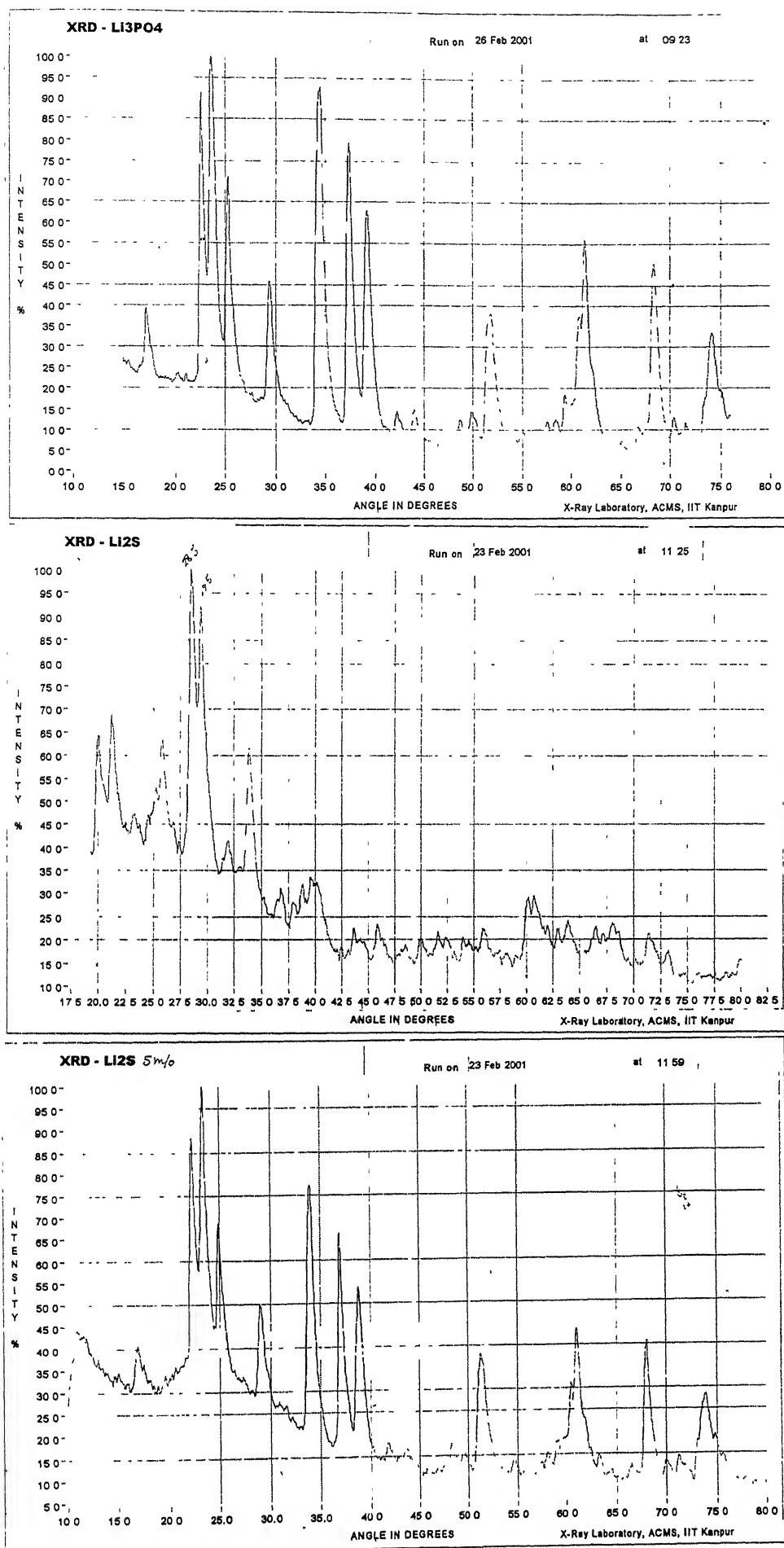


Fig 3.1: XRD patterns for Li_3PO_4 , Li_2S 5m/o Li_2S Composition

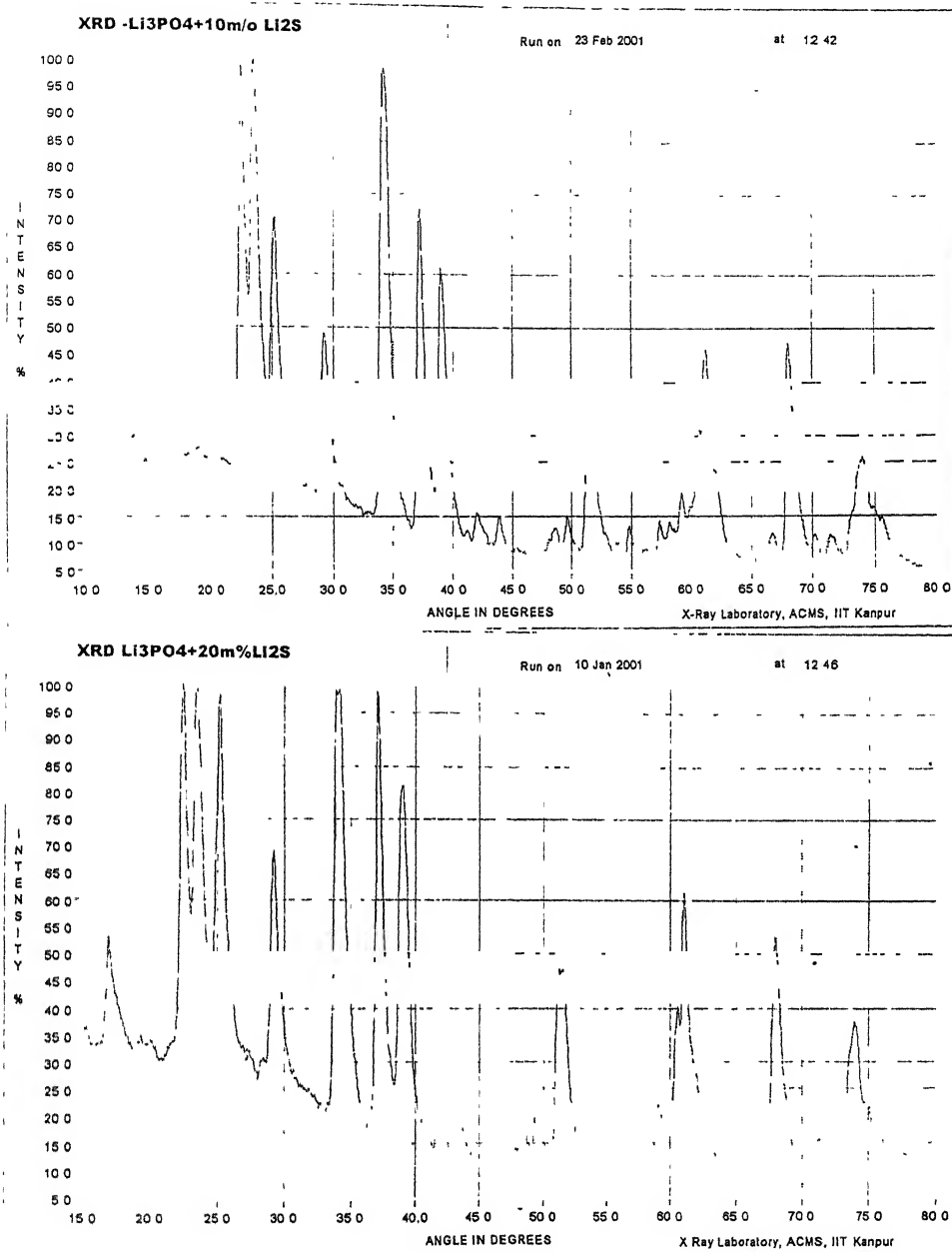


Fig 3.2: XRD patterns for 10, 20 m/oLi₂S Composition

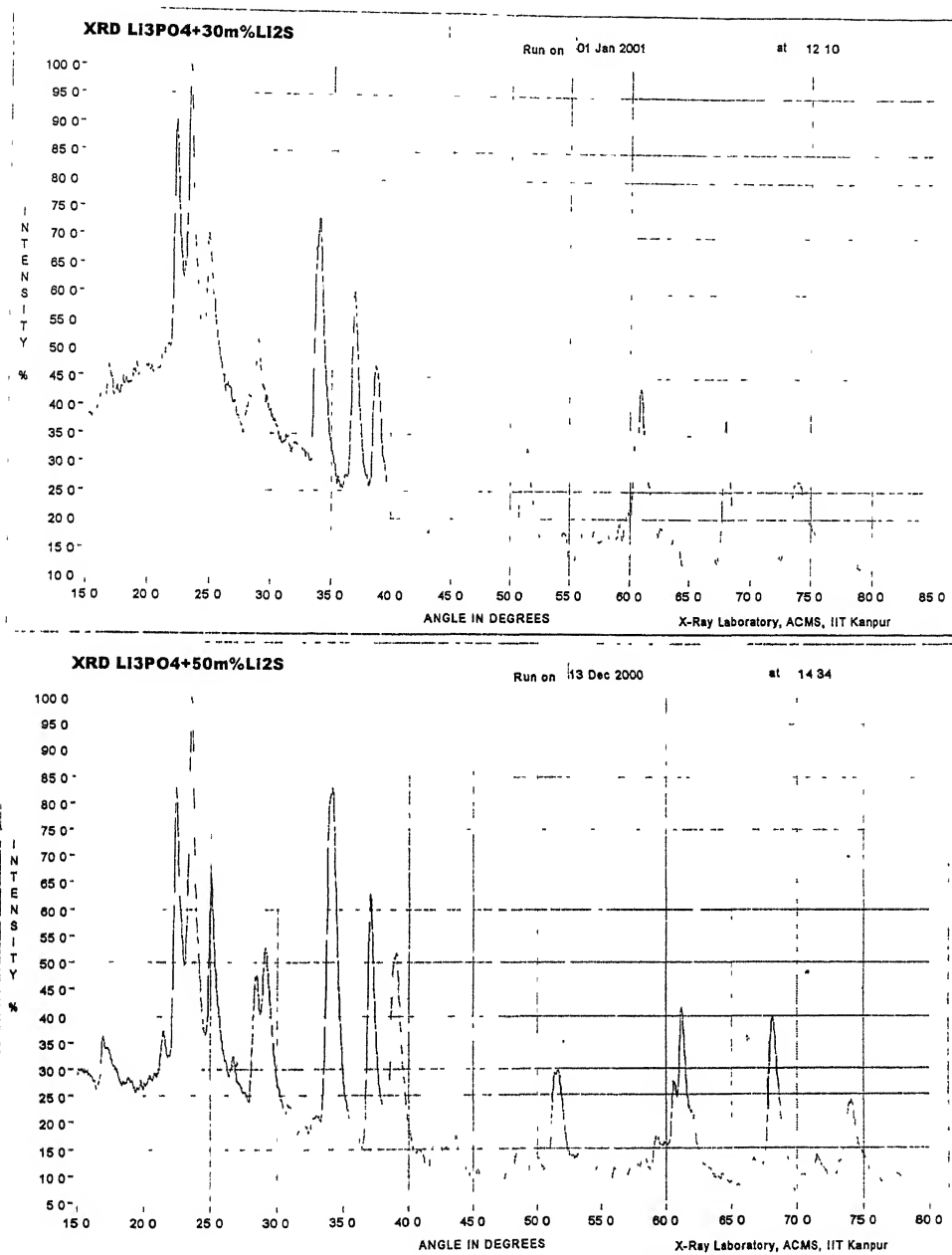


Fig 3.3: XRD patterns for 30, 50m/oLi₂S Composition

3.2.2 Milled Samples

XRD patterns have been recorded for samples before milling and each after an interval of every 10 hours of milling. All the XRD patterns have been recorded at room temperature. Some of these results are presented in Fig. 3.4-3.6 for 20, 30 and 50 m/o Li_2S samples. In Fig. 3.4 XRD patterns (for 20m/o Li_2S composition) without milling, 73 hours of milling and 135 hours of milling have been presented, it is clear from the recorded patterns that all the major peaks have shown a decrease in the height after 73 hrs of milling and a further decrease after 135 hrs of milling. Since even after 135 hours peaks are not disappeared therefore it can be concluded that after 135 hrs of milling, the system under experimentation haven't loosen its crystalline nature though particle size is expected to be reduced. Similar results are observed for 30 and 50 m/o Li_2S composition, which have been milled for 188 and 71 hrs respectively. The reason for different hours of milling for different compositions was that no reduction in peaks has been observed for several hours of milling and therefore samples have been not milled further. Each of these Figures compares the XRD results for the freshly prepared mixtures as with those for mixtures, which were ball milled for many hours.

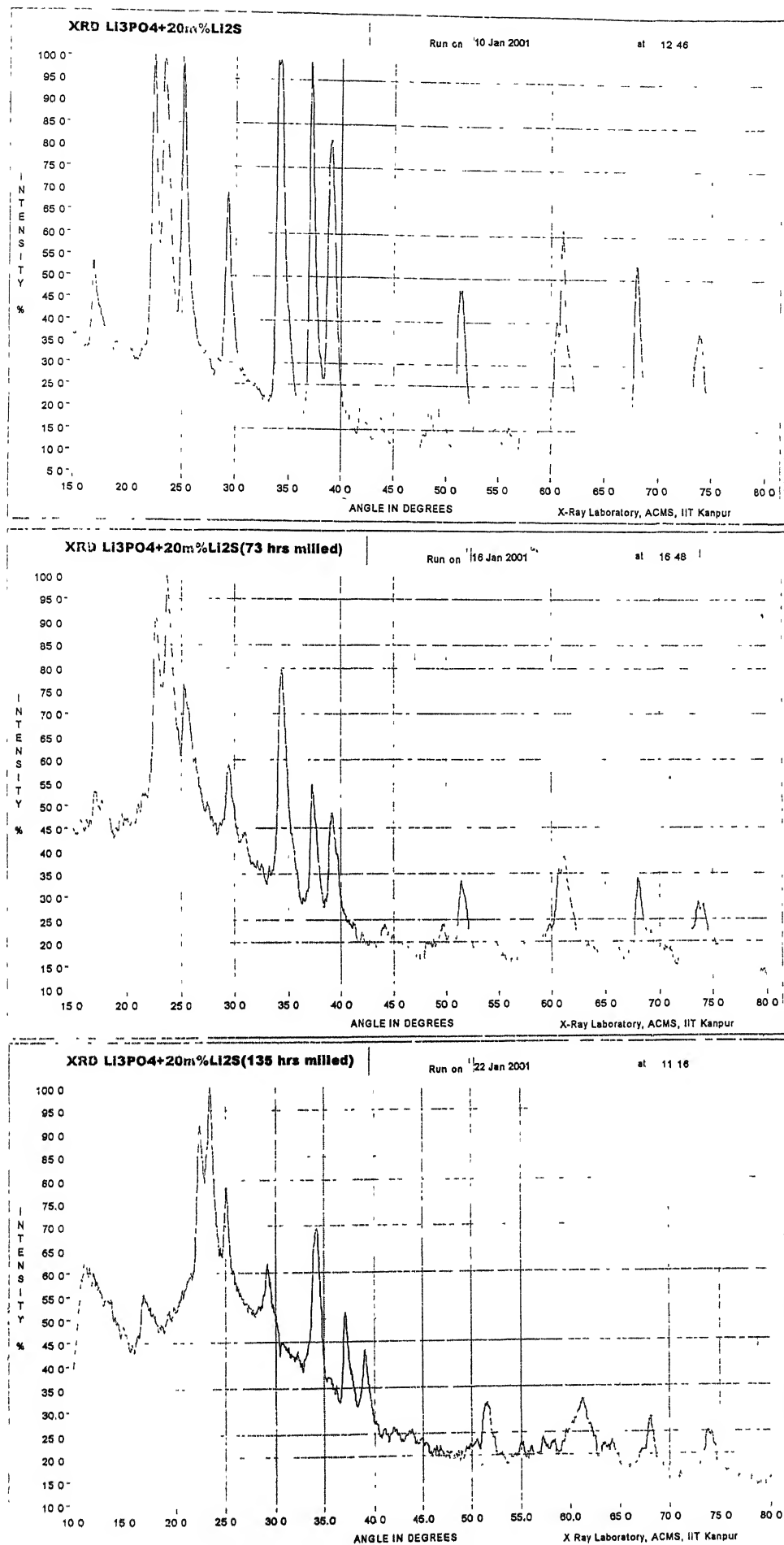


Fig 3.4 XRD patterns for the 0, 73, 135 hours milled samples of composition 20m/o

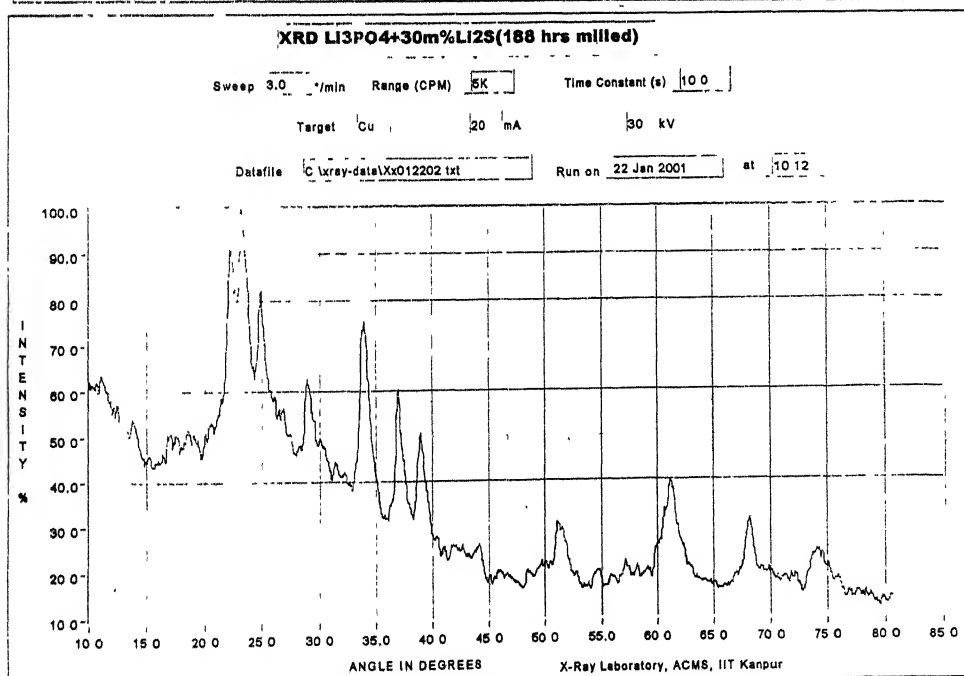
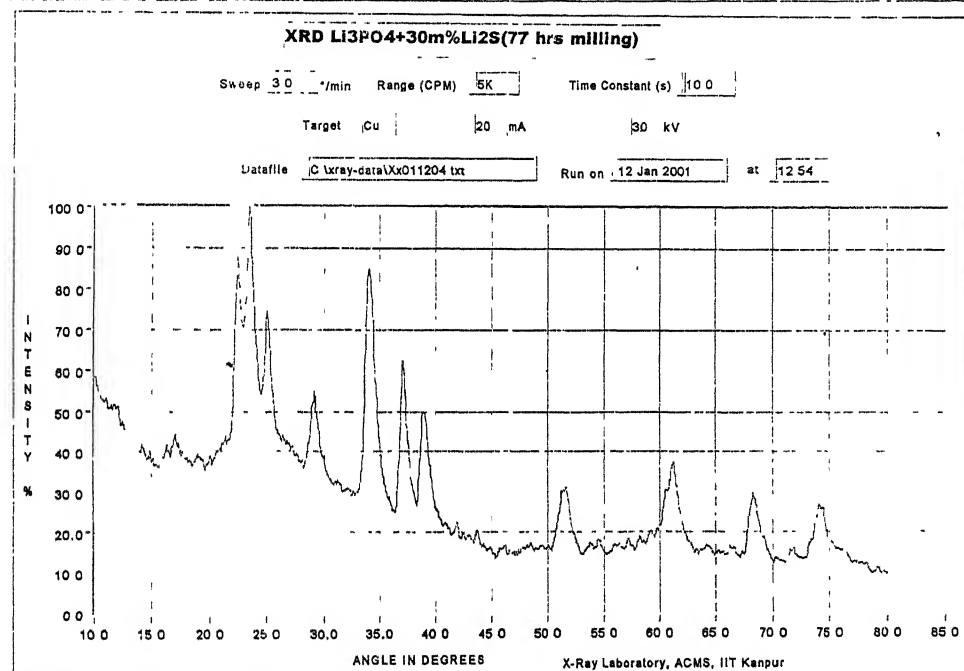
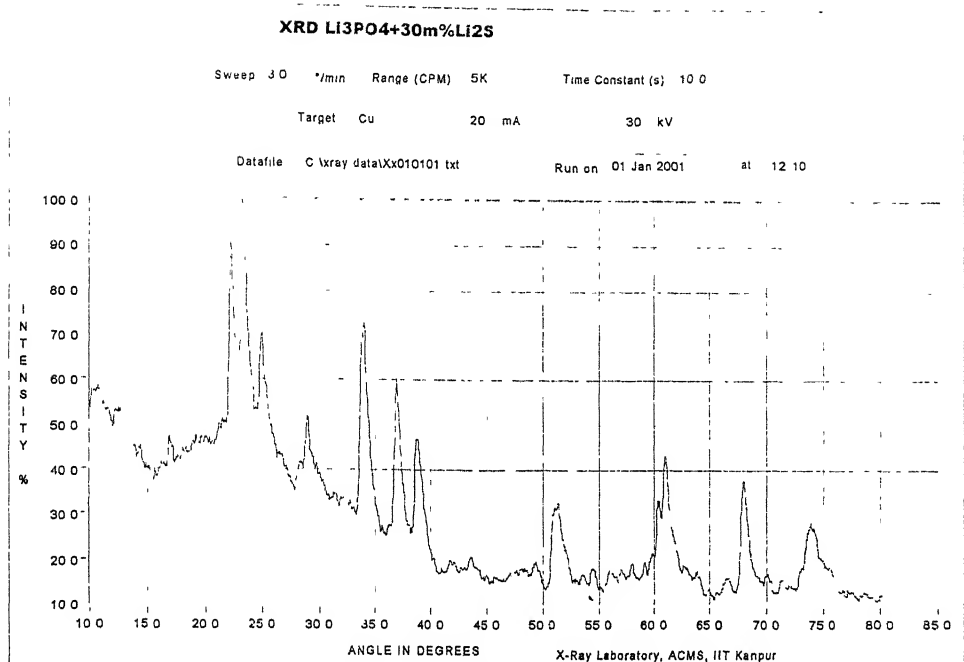


Fig 3.5 XRD patterns for the 0, 77, 188 hours milled samples of composition 30m/o

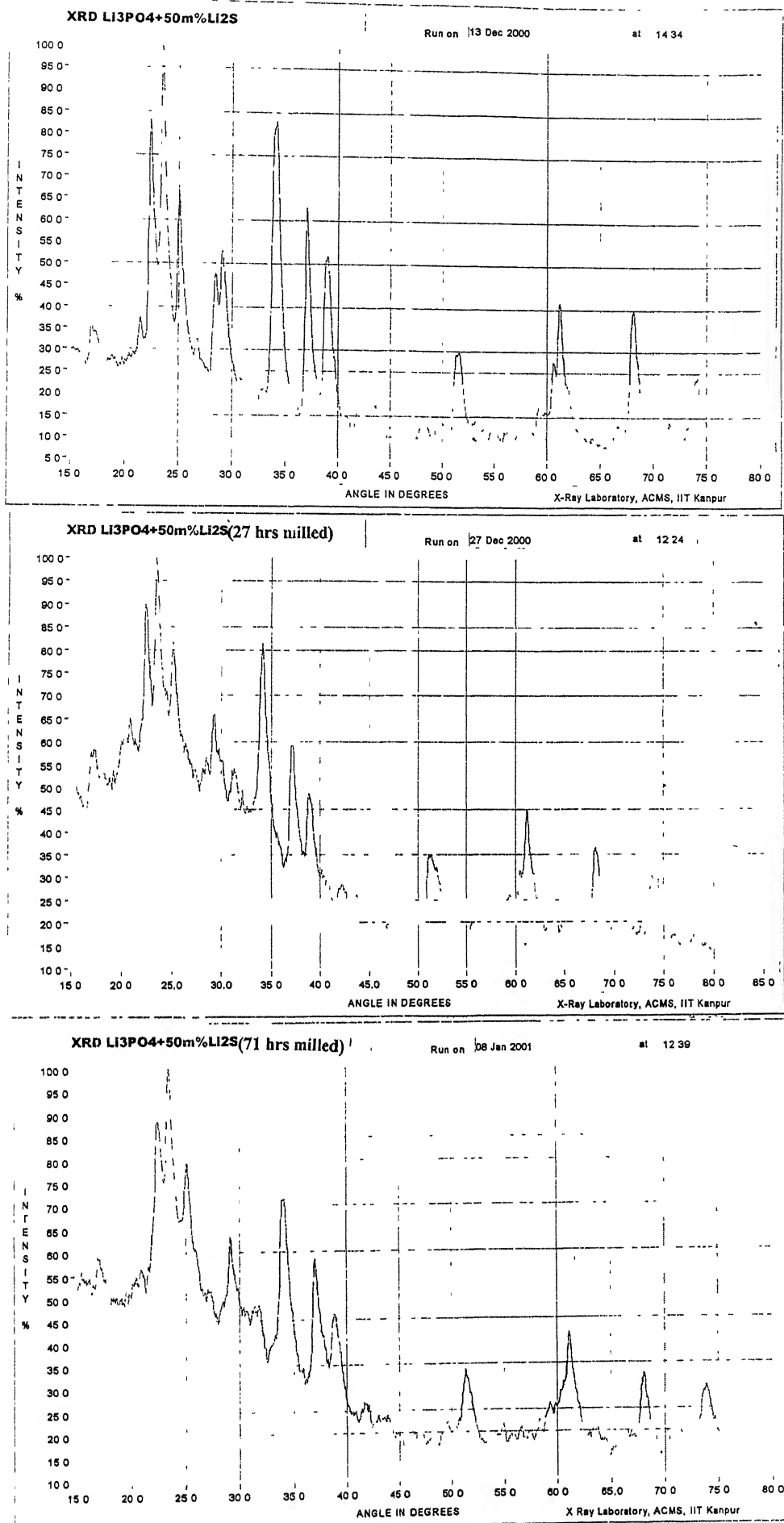


Fig 3.6 XRD patterns for the 0, 27, 71 hours milled samples of composition 50m/o

3.3 Impedance analysis

3.3.1 Conventional Sample

The complex impedance Z^* consists of real and imaginary parts Z' and Z'' . A plot of Z'' vs. Z' with a frequency variation, popularly known as impedance plot, which not only facilitates the modelling of the electrolyte/electrode assembly in terms of electrical components (e.g. resistor, capacitor, etc.) but also directly provides the dc resistance of the sample. The electrolyte impedance is the dominating term in Z^* , though it consists of electrolyte, electrode, and connecting lead impedances.

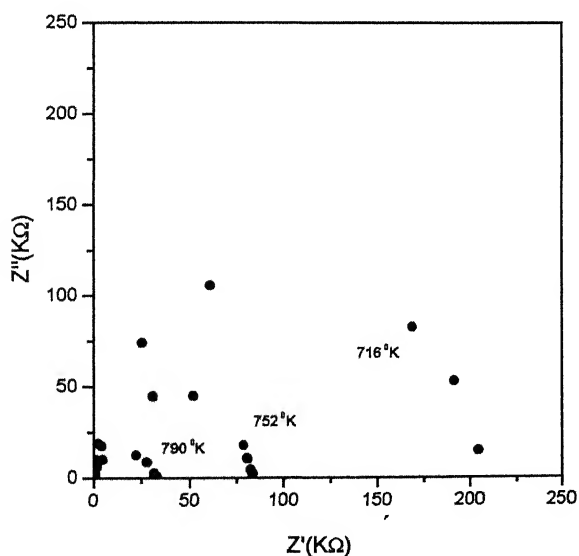


Fig. 3.7 (a): Impedance plot for Li_3PO_4 at 716, 752, 790 °K

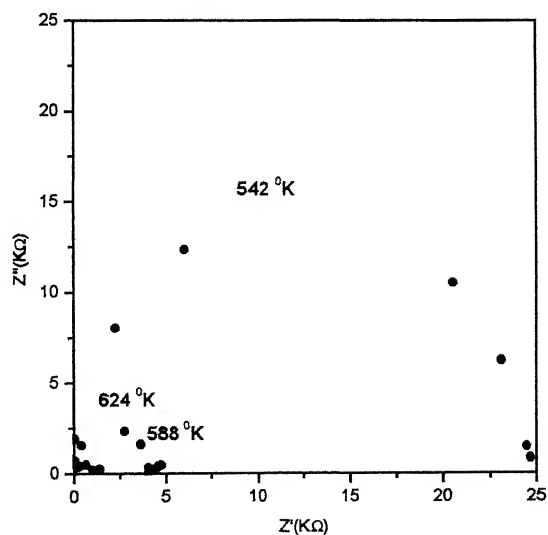


Fig. 3.7 (b): Impedance plot for Li_2S at 542, 588, 624 °K

Figs.3.7(a-b) show the impedance plots at different temperatures for the pure starting materials Li_3PO_4 and Li_2S , which are reasonably good semicircles, within experimental error, in all the cases. As discussed in section 2.6.2, these samples can be modeled as parallel combination of a resistor and a capacitor, and their dc resistances can be obtained from the diameter of the semicircle.

As clearly visible in Figs. 3.7(a-d), on increasing the temperature the diameter of the semicircle, which is indicative of the dc resistance R_{dc} of the sample, decreases. It is in conformity with the fact that conductivity of ionic solids increases on increasing the temperature, the reason is that at higher temperature the ions are having more energy to cross energy barrier so as to reach to another site and as a result ionic conductivity increases.

The impedance plots shown in Fig. 3.7(b) and Fig. 3.8 also exhibit a straight line behaviour at lower frequencies which signifies presence of electrolyte/electrode

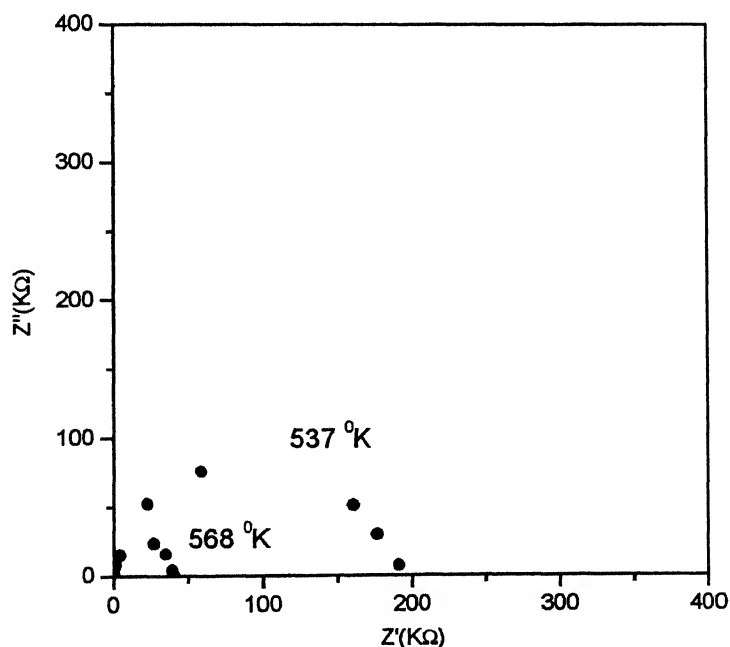


Fig. 3.7 (c): Impedance plot for 30m/o composition at 537, 568 °K

interfacial capacitance and also gives an idea about the smoothness of the surface (see section 2.5). A straight line at 90° is obtained for perfectly smooth surfaces and the slope decreases as roughness increases.

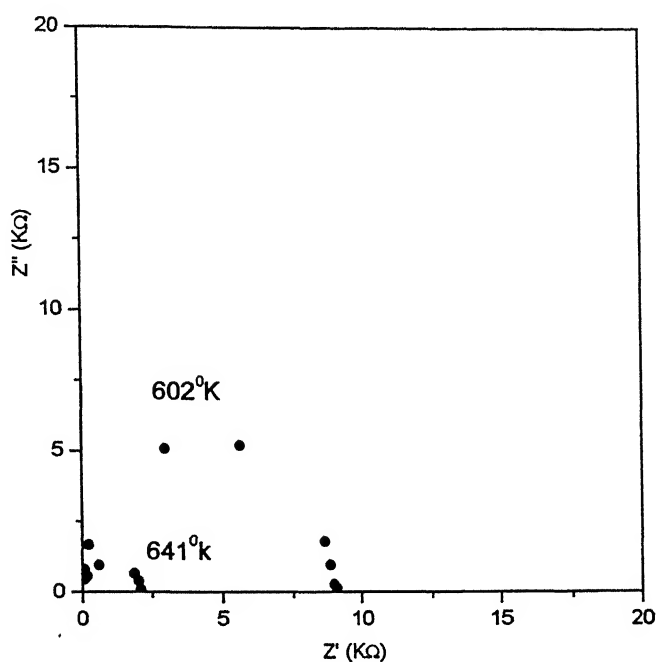
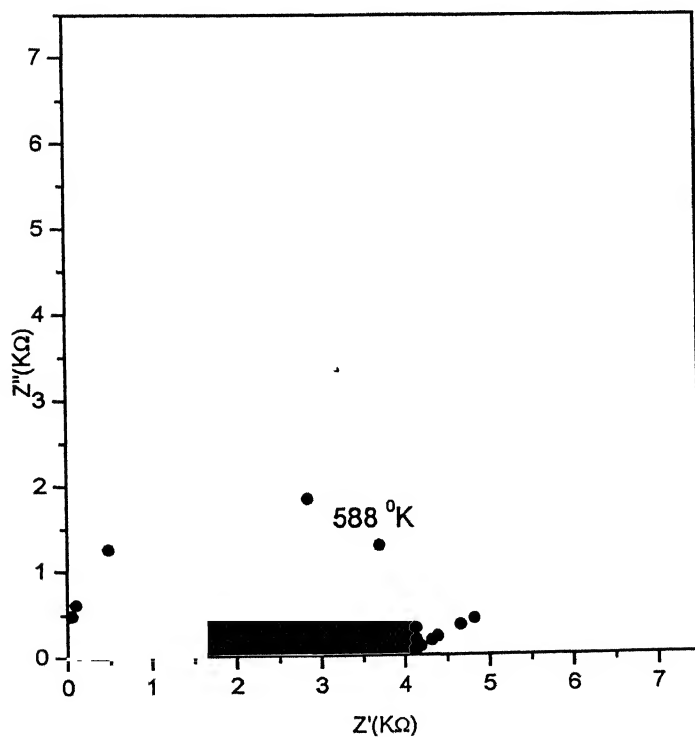


Fig. 3.7 (d): Impedance plot for 30 m/o Li_2S composition at 602, 641 °K



3.3.2 Milled Sample

The impedance plots for the ball-milled and the normal samples of 20m/o

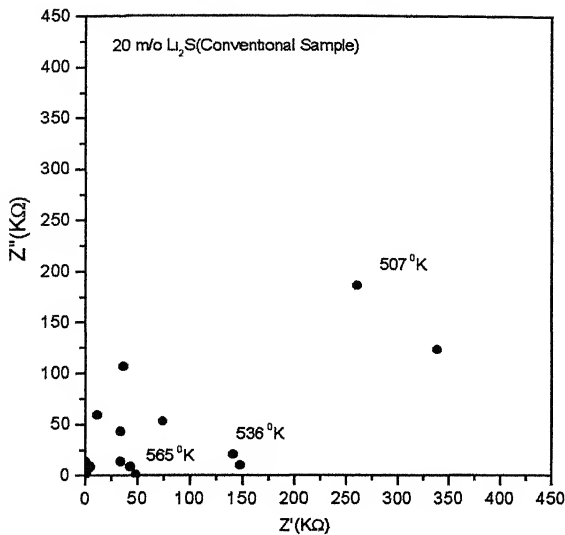


Fig. 3.9(a): Impedance plot for 20 m/o Li_2S composition (conventional) at 507, 536, 565 $^{\circ}\text{K}$

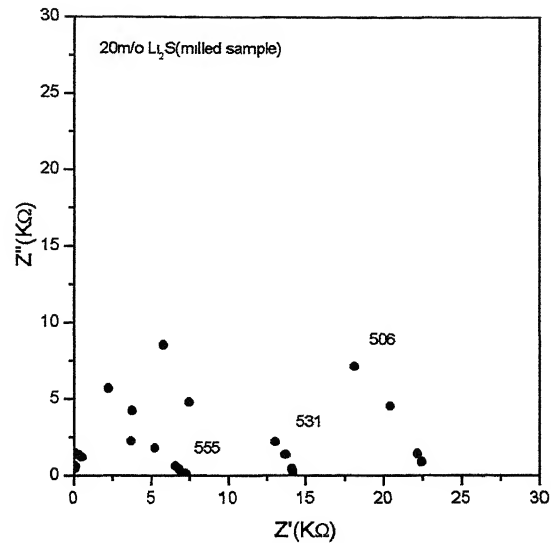


Fig. 3.9(b): Impedance plot for 20 m/o Li_2S composition (milled) at 506, 531, 555 $^{\circ}\text{K}$

Li_2S composition at three different temperatures are shown in Fig.3.9. As is evident from these results, the impedance plots are semicircles. From Fig.3.9 (b), the dc resistance shown by the 20m/o Li_2S composition at 506 $^{\circ}\text{K}$ is around 22.5 k Ω (diameter of the semi-circle). Since no qualitative change in the impedance plot for ball-milled sample is observed, these samples can also be modeled as an electrical circuit with a resistor and capacitor in parallel.

3.4 DC Conductivity

The semicircular impedance plots are used to find the dc resistance of the sample. Their diameters directly give the values of dc resistance of the sample. Basically complex impedance measured using impedance analyzer is the combination of the electrolyte (sample), electrode and the connecting leads, but the

impedance of the sample is dominating so Z^* is considered as the impedance of the sample only. The dc conductivity is given by the relation:

$$\sigma_{dc} = \frac{l}{R_{dc}A}$$

Where l is the thickness, A the cross sectional area R_{dc} the dc resistance of the sample. Whenever the semicircular impedance plots are not obtainable within the test frequency range (5Hz-13MHz), the $Z/\cos\theta$ has been used as dc resistance (in accordance with the concept detailed in section 2.6). It is observed that conductivity vs. inverse of temperature dependence follows Arrhenius law. Two slopes are observed for Li_3PO_4 , $\text{Li}_3\text{PO}_4+70\text{m/o Li}_2\text{S}$ and Li_2S samples. An increase in dc conductivity is observed with an increase in temperature. At higher temperatures steep increase in conductivity is observed.^[21]

3.5 Conductivity vs. composition

3.5.1 Conventional Samples

The log dc conductivity vs. inverse temperature plots for eight different compositions are shown in Fig. 3.10. The conductivity plots for three ball-milled compositions have been discussed in the next section.

A “regular” variation of the conductivity as a function of composition is observed for $x\text{Li}_3\text{PO}_4-(1-x)\text{Li}_2\text{S}$ system under investigation. It is observed that the conductivity increases with increasing m/o of Li_2S in $\text{Li}_3\text{PO}_4\text{-Li}_2\text{S}$ system. Similar type of behaviour is also shown by $\text{Li}_2\text{S-LiBr}$ system, in which conductivity increases with increasing mole fraction of LiBr .^[22]

A steep increase in the conductivity is observed for almost all the compositions except pure Li_3PO_4 , 5 and 10m/o Li_2S compositions. Since Li_2S starts melting at around 550°C , the steep change in the conductivity may be attributed to

the presence of relatively high conducting Li_2S liquid phase in the solid phase (Li_3PO_4).

According to the Maxwell's model for composites as discussed earlier in section 1.6, the conductivity of a composite electrolyte consisting of two constituents is given by the relation;

$$\sigma_{\text{composite}} = f_1\sigma_1 + f_2\sigma_2$$

Where f_1 and f_2 are the mole fractions and σ_1 and σ_2 are the conductivities of the two constituents. The electrical conductivities values are calculated using the above equation at 713°K . These along with the experimental values are given in Table 3.1. The following values of the conductivities of the two components (Li_3PO_4 and Li_2S) are used in the above calculation.

$$\sigma_{\text{Li}_3\text{PO}_4 (\text{at } 713^\circ\text{K})} = 1.9 \times 10^{-6} \Omega^{-1} \text{cm}^{-1}$$

and

$$\sigma_{\text{Li}_2\text{S} (\text{at } 713^\circ\text{K})} = 5.1 \times 10^{-3} \Omega^{-1} \text{cm}^{-1}$$

Table 3.2: Observed and calculated values of conductivities of $\text{Li}_3\text{PO}_4\text{-xLi}_2\text{S}$ system at 713⁰K for different compositions.

Composition(x) (m/o)	Observed σ_{dc} ($\Omega^{-1}\text{cm}^{-1}$)	Calculated σ_{dc} using Maxwell model($\Omega^{-1}\text{cm}^{-1}$)
0	1.9×10^{-6}	---
5	1.0×10^{-5}	2.6×10^{-4}
10	1.1×10^{-4}	5.1×10^{-4}
20	4.3×10^{-4}	1.0×10^{-3}
30	8.7×10^{-4}	1.5×10^{-3}
50	1.5×10^{-3}	2.6×10^{-3}
70	1.9×10^{-3}	3.6×10^{-3}
100	5.1×10^{-3}	---

It is evident from Table 3.2 that the calculated and observed values differ by an order of magnitude for 5m/o Li_2S and thus it is concluded that the system under consideration does not satisfy the Maxwell model(the law of average conductivity).

The enhancement in the conductivity may be reconciled in view of the XRD results. The 5m/o Li_2S sample has a maximum enhancement in conductivity by around one order of magnitude. The 10m/o Li_2S sample exhibit an enhancement of much less than an order of magnitude. It is possible that the solubility of Li_2S in Li_3PO_4 is limited between 5 and 10 m/o Li_2S . Similarly for 20 m/o Li_2S sample, a part of Li_2S a part goes into solid solution and therefore for these three compositions (5, 10 and 20m/o Li_2S) appreciable enhancement in conductivity is observed. The 30, 50 and 70m/o $\text{Li}_2\text{S-Li}_3\text{PO}_4$ samples have largely two-phase mixtures and therefore enhancement in conductivity is limited.

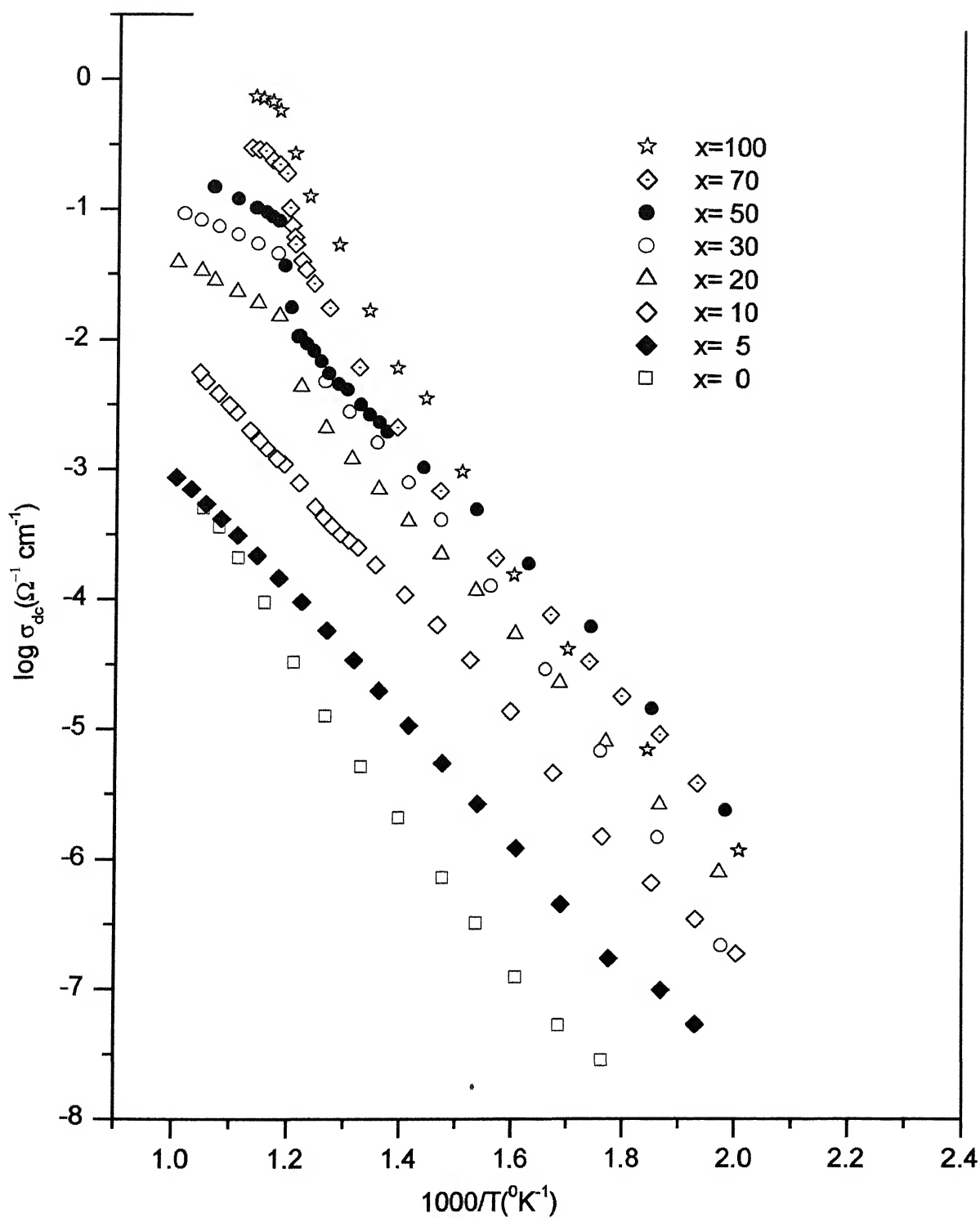


Fig. 3.10: Log conductivity vs. inverse temperature plot for $\text{Li}_3\text{PO}_4\text{-}x$ m/o Li_2S system

3.5.2 Ball-Milled Samples

The dc conductivity vs. inverse of temperature plots for 20,30 and 50 m/o Li_2S ball-milled samples and the conventional samples are presented in Figs. 3.11,3.12 and Fig. 3.13 respectively. An increase in the conductivity after milling is reported for all the three 20m/o, 30m/o and 50m/o Li_2S composition. For 20 and 30m/o Li_2S this enhancement in conductivity, however is not uniform at all temperatures. At lower temperatures the enhancement in the conductivity is more than that at high temperatures, where it is comparable with conventional sample without milling. A maximum enhancement of about 15 times at lower temperatures is observed for 20m/o Li_2S composition. The results for 30m/o Li_2S composition are quite similar to that of 20m/o Li_2S composition Figs. 3.11-3.12. An another composition that was synthesized using ball-milling was 50m/o Li_2S , and in this case also a conductivity enhanced by almost an order of magnitude was observed. Moreover, this enhancement in conductivity for this sample is almost same at all the temperatures.

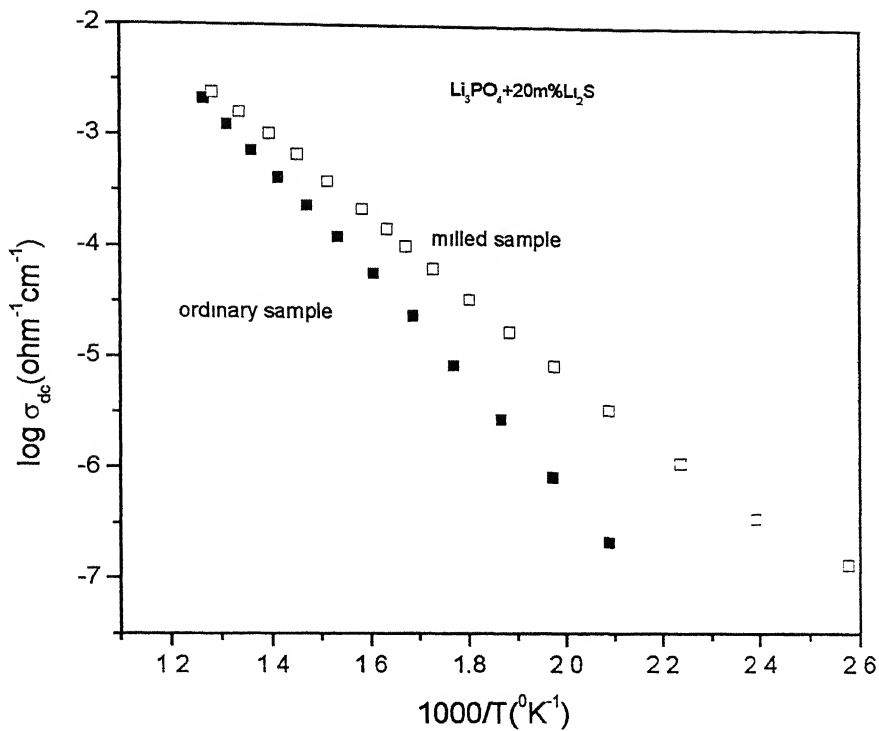


Fig. 3.11: Log conductivity vs. inverse temperature plot for ordinary and milled (135hrs.) samples of 20m/oLi₂S composition

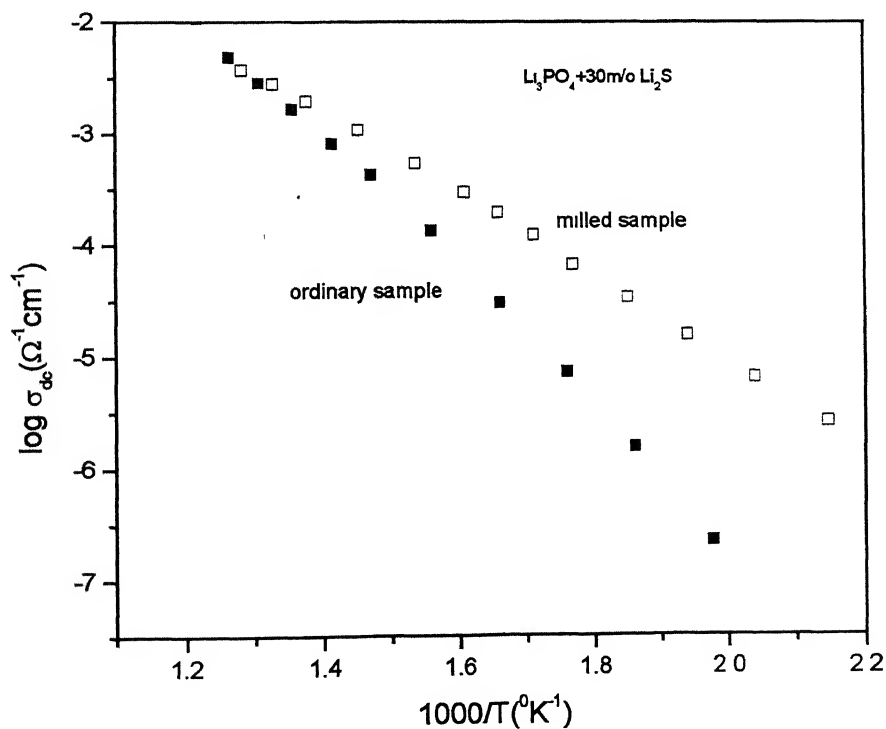


Fig 3.12: Log conductivity vs. inverse temperature plot for ordinary and milled (188hrs.) samples of 30m/oLi₂S composition

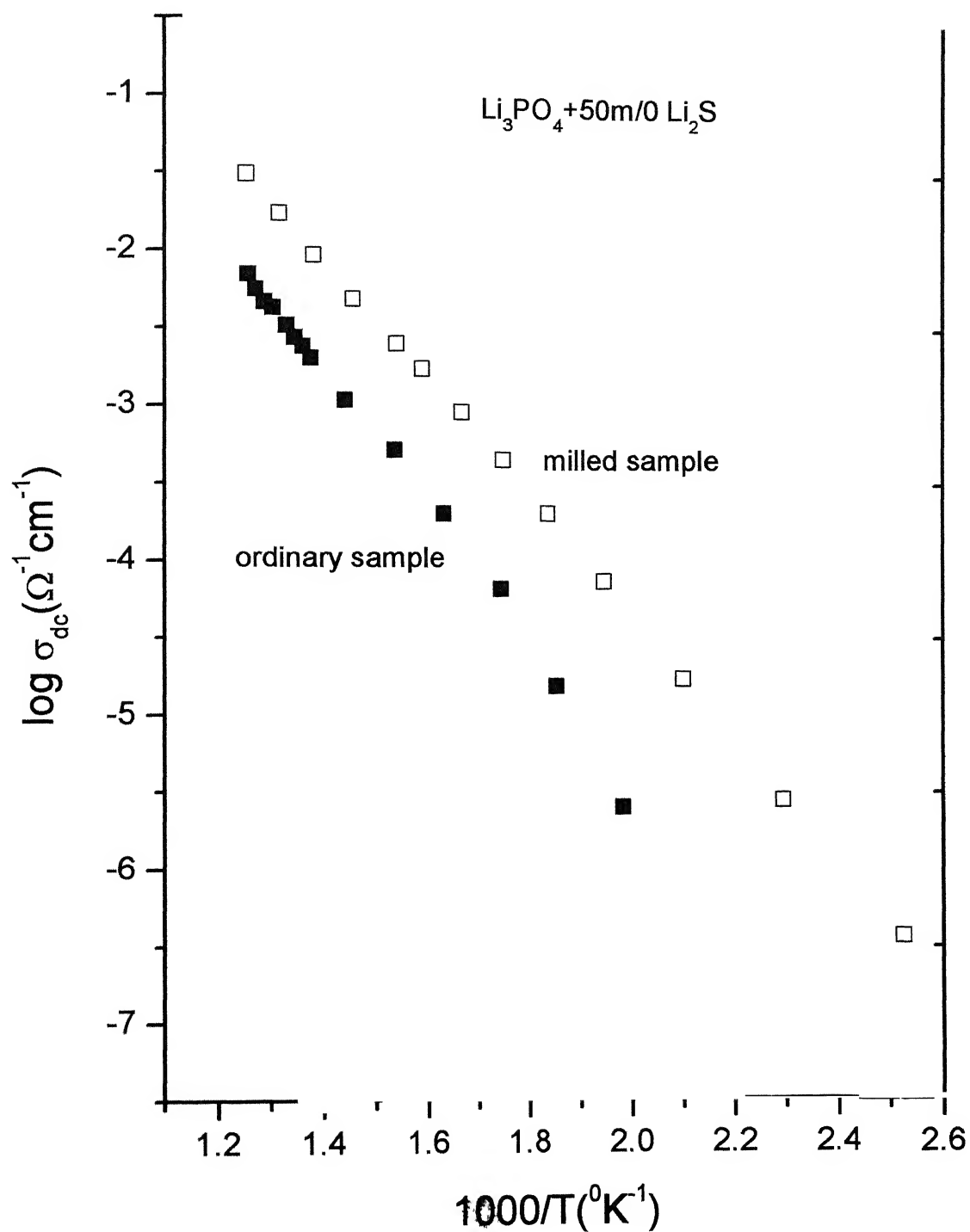


Fig. 3.13: Log conductivity vs. inverse temperature plot for ordinary and milled (71hrs.) samples of 50m/o Li_2S composition

3.6 Analysis of dielectric moduli

As discussed earlier in section 1.5 real(M') and imaginary(M'') parts of complex modulus M^* can be represented in the terms of f , Z and θ :

$$M' = \omega C_0 Z \sin \theta$$

$$M'' = \omega C_0 Z \cos \theta$$

Using these equations M' and M'' of the complex dielectric modulus M^* have been evaluated for all the compositions. Origin software is used for sigmoidal

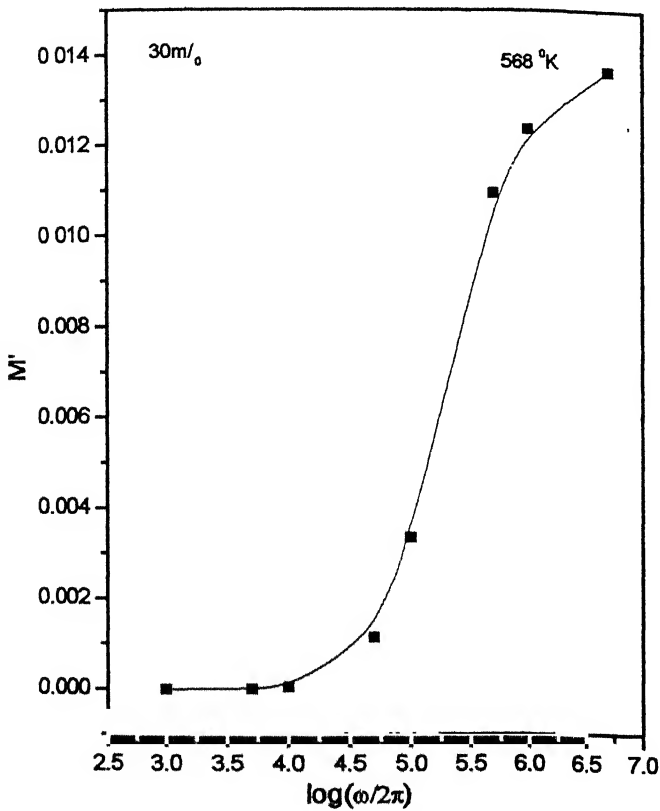


Fig. 3.14(a): Modulus (M') spectra at 537 °K for 30m/o Li_2S composition

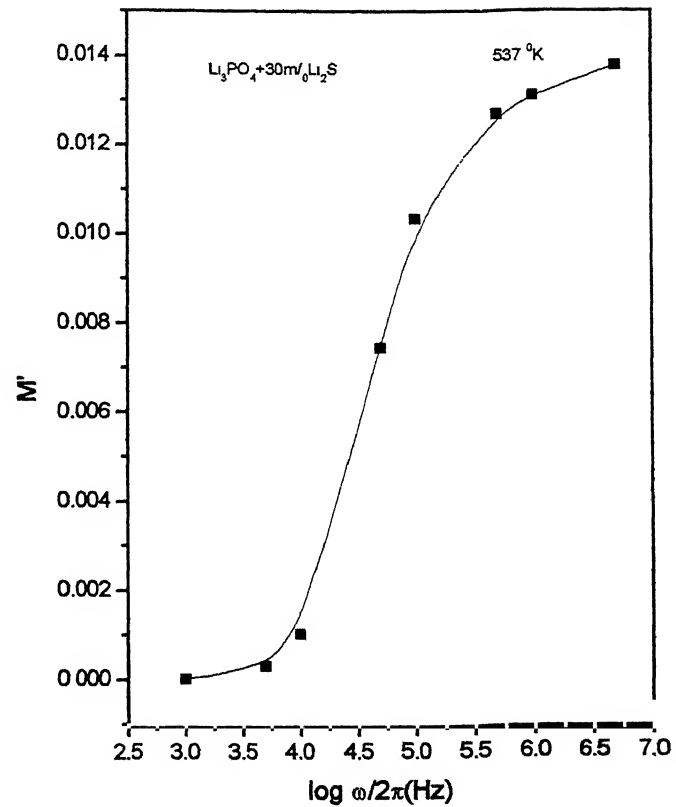


Fig. 3.14(b): Modulus (M') spectra at 568 °K for 30m/o Li_2S composition

curve fitting of M' vs. $\log(\text{frequency})$ curve and Lorentzian curve fitting for M'' vs. $\log(\text{frequency})$ curve. Variation of M' with $\log(\text{frequency})$ for different samples have been presented in Fig. 3.14(a-b), as it is well known that the bulk dielectric

behaviour is highlighted and the interfacial effects tend to be eliminated in the modulus form of representation. As expected, the M' values tend towards zero at lower frequencies and level off at higher frequencies in usual sigmoidal fashion. However, as the maximum frequency is 13MHz sometimes the leveling off was not observable in our studies and thus M' seems to ever increasing.

Similarly variation of M'' as a function of $\log(\text{frequency})$ for different compositions at different temperatures is presented in Fig.3.15 (a-f). Relaxation peaks were observed in all the systems within different temperature ranges. At some temperatures relaxation peaks are not observable because of the limited variation in frequency from 5Hz to 13MHz. The peaks in the M'' vs. $\log(\text{frequency})$ plots signify the presence of relaxation processes. For all the compositions (0,5,10,20,30,50,70,100 m/o Li_2S) in this work, the height of the relaxation peaks increases with increasing the temperatures. Further, the height of the peak, at a

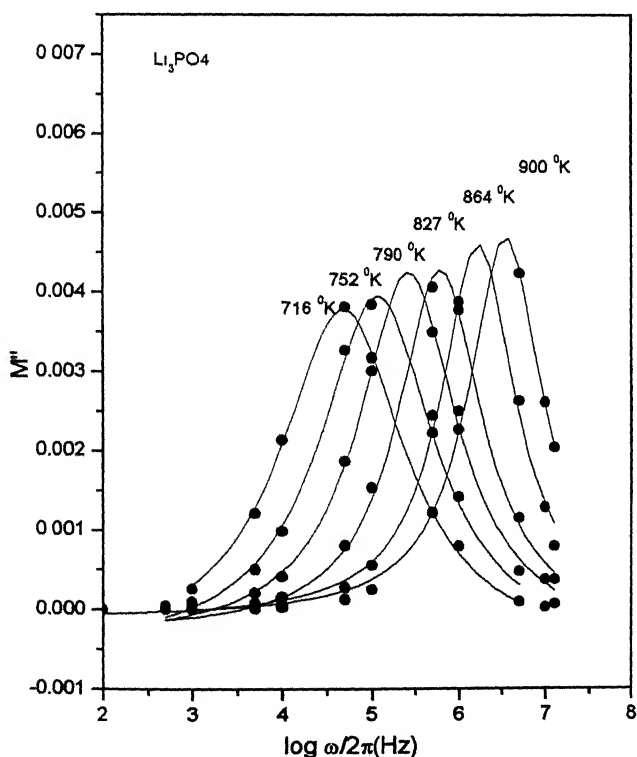


Fig. 3.15(a): Modulus spectra (M'') at different temperatures 716,752,790,827,864,900 °K for pure Li_3PO_4 composition

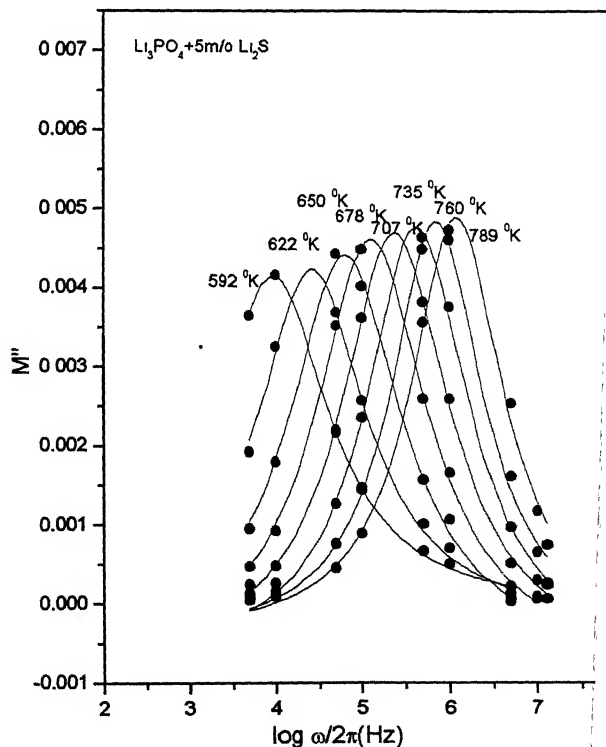


Fig. 3.15(b): Modulus spectra (M'') at different temperatures 592,622,650,678,707,735,760, for 5m/o Li_2S composition

certain temperature is increases as the concentration of Li_2S in Li_3PO_4 increases. Mangion and Johari have reported that AgI-AgPO_3 glassy system shows a slight increase in M'' height with increase in the temperature.^[23] It is clear from Fig. 3.15(a-f) that relaxation frequency shifts to higher values as temperature increases.

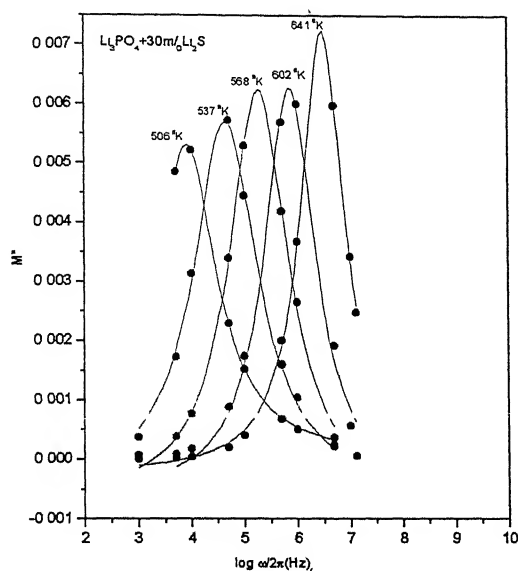


Fig. 3.15(c): Modulus spectra (M'') at different temperatures 506,537,568,602,641 °K for 30m/o composition

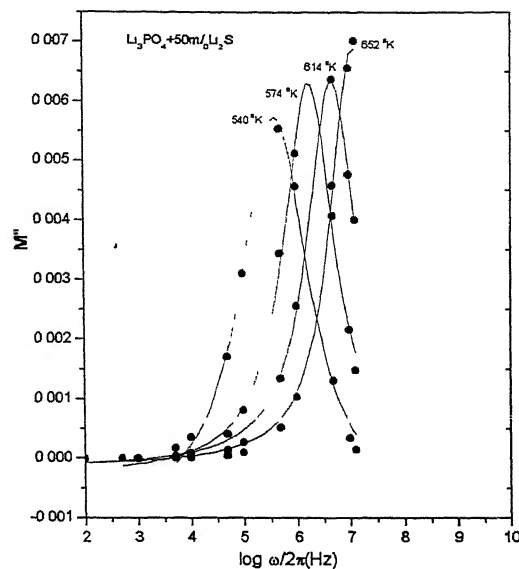


Fig. 3.15(d): Modulus spectra (M'') at different temperatures 540,574,614,652 °K for 50m/o composition

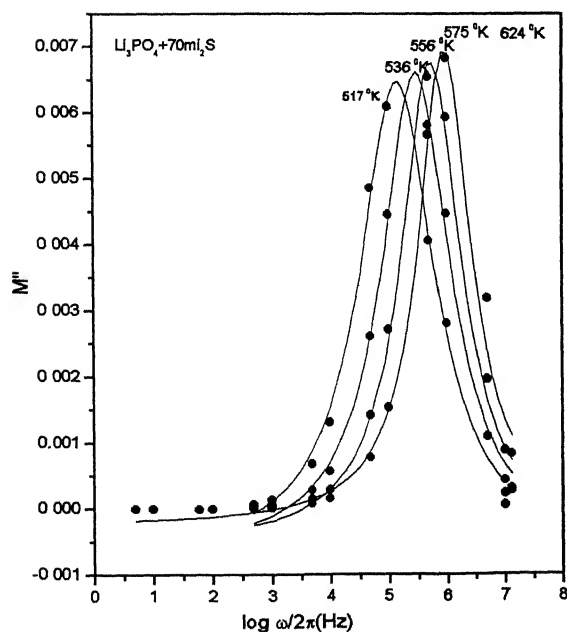


Fig. 3.15(e): Modulus spectra (M'') at different temperatures 517,536,556,575,652 °K for 70m/o Li_2S composition

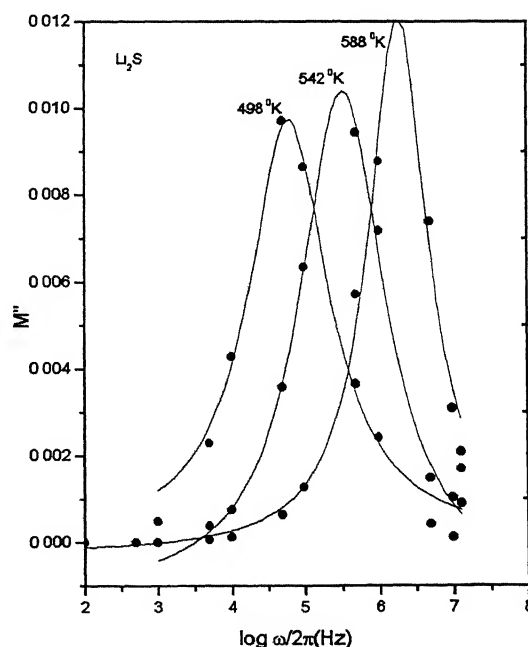


Fig. 3.15(f): Modulus spectra (M'') at different temperatures 498,542,588 °K for Li_2S

The relaxation time at 496 °C has been extracted for all the conventionally prepared samples . The relaxation frequency ω_r at a particular temperature has been obtained from the $\log(\omega_r / 2\pi)$ vs. $1000/T$ plots (here ω_r has been derived from M'' vs. $\log(\omega_r / 2\pi)$ plot). The relaxation time τ and the relaxation frequency (ω_r) are related by:

$$\tau = 2\pi / \omega_r$$

The relaxation times for all conventionally prepared eight compositions at 496°C have been listed in Table 3.3. The relaxation time is maximum for the lowest conducting composition and is minimum for the highest conducting composition.

Table 3.3: Relaxation times for 0, 5, 10, 20, 30, 50, 70 and 100m/o Li₂S compositions at 496°C

Composition (m/o)	$\log(\omega_r / 2\pi)$ (Hz)	Relaxation time τ_r (sec)
0	5.25	3.5E-5
5	5.91	7.7E-6
10	7.53	1.9E-7
20	7.52	1.9E-7
30	8.07	5.4E-8
50	8.14	4.7E-8
70	7.98	4.1E-8
100	8.27	3.4E-8

Since the plots of M'' vs. \log frequency shown in Fig. 3.5(a-f)) are symmetric with respect to the peak maxima, it can be predicted that a single dielectric relaxation process is dominating^[24,25] It was earlier concluded from the activation energy comparison that the conductivity is the dominating relaxation process in Li₃PO₄-

Li_2S system. Therefore these results are supporting each other and lead to the confirmation of concluding remark that only conductivity relaxation process dominates in the system under consideration.

Figs. 3.16(a-c) are the typical plots of M' and M'' vs. \log frequency. As the source frequency approaches the relaxation frequency (ω_r), M' starts increasing rapidly and then attains a saturation value while M'' exhibits a well defined peak. These results, Fig. 3.16(a-c), are as expected for systems with characteristic relaxation process.

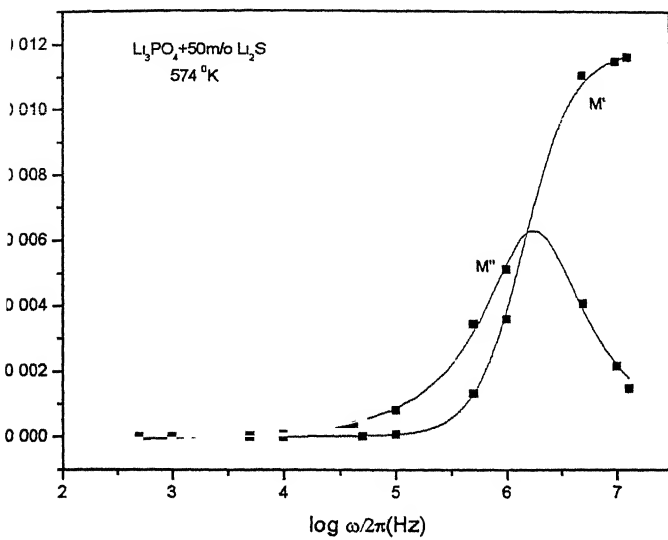


Fig. 3.16 (a): M'/M'' dependence on frequency

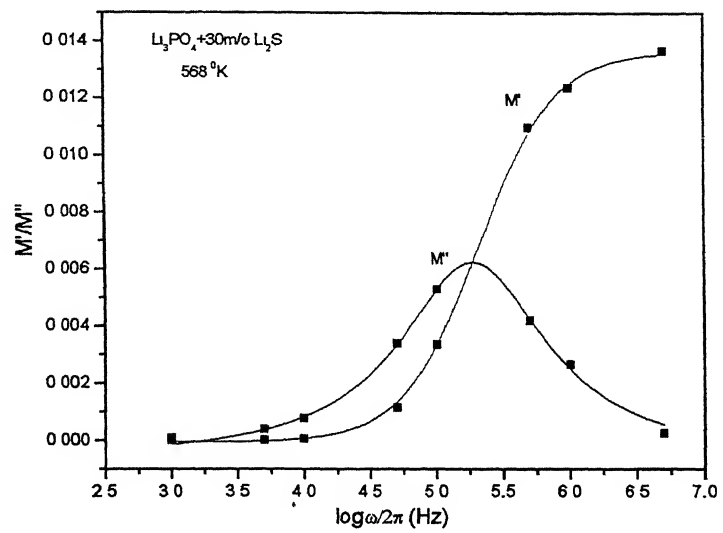


Fig. 3.16 (b): M'/M'' dependence on frequency

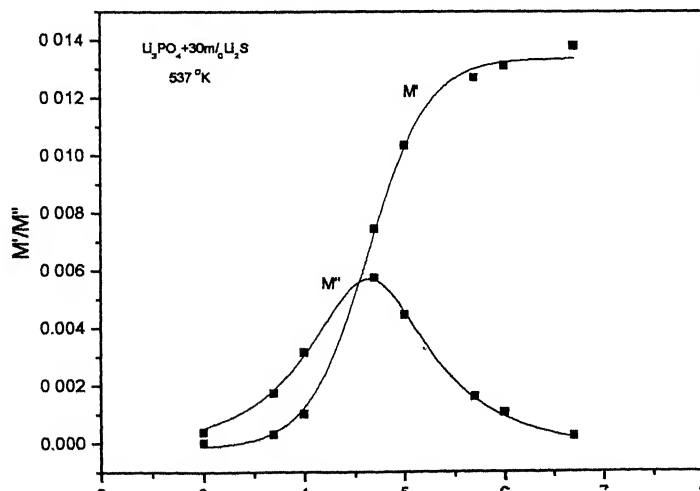


Fig. 3.16 (c): M'/M'' dependence on frequency

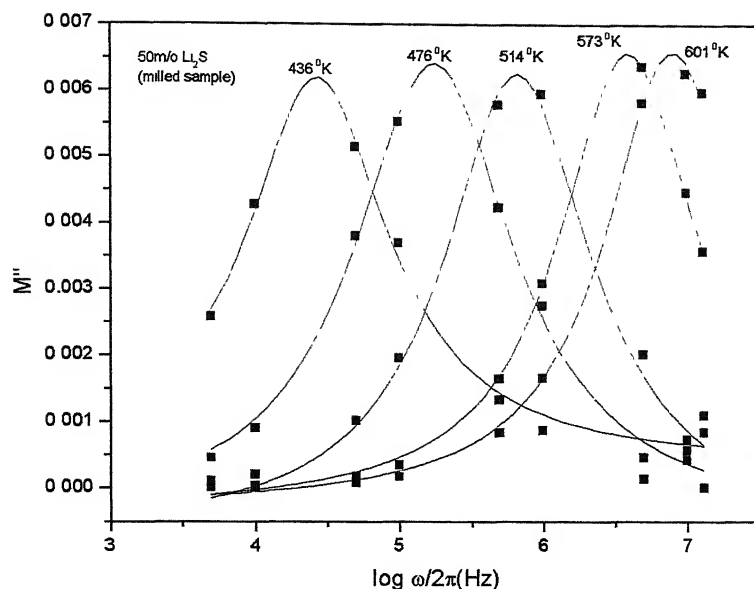


Fig. 3.17: Modulus spectra (M'') at different temperatures 436,476,514,573 and 601 °K for 50m/o Li_2S (milled) composition

Fig. 3.17 shows the M'' vs. log frequency plot at different temperatures for 50m/o Li_2S milled system. The well defined peaks of nearly equal height are the characteristics of the relaxation process.

3.7 Activation Energy-A Comparison(Conventional samples)

As discussed in section 1.4, the slope of the log conductivity vs. inverse temperature plot is a measure of the activation energy. Only three compositions viz. 0m/o, 70m/o and 100m/o Li_2S display two different slopes in their $\log \sigma - 1/T$ plots(Fig. 3.10). The activation energies for all the samples have been extracted and these are listed in the Table 3.4. This activation energy corresponds to the conductivity process only. Basically the observed electrical relaxation associated with long range diffusion and conduction processes is referred to as “conductivity

relaxation” to distinguish it from dielectric relaxation involving dipole reorientation, which is termed as “dipolar relaxation”.^[26]

Another way to find activation energy is to extract the relaxation frequency from M'' vs. $\log(\omega/2\pi)$ plot and draw $\log \omega_r$ vs. $1000/T$ plot, which comes out as a straight line. The slope of this line yields another activation energy associated with the dielectric processes. This activation energy acknowledges all the relaxation processes occurring in the system under consideration. It is very clear from the Table 3.4 that the activation energies (E_a) derived from conductivity plots and $\log(\omega/2\pi)$ vs. inverse of temperature plots are same within the limits of the experimental error and possible percentage error in linear fitting. Therefore it is safely concluded that the conduction mechanism is the dominating process for the dielectric relaxation, as well.

Table 3.4 Comparison of activation energies obtained from temperature dependence of conductivity and relaxation frequency plots for $\text{Li}_3\text{PO}_4\text{-xLi}_2\text{S}$

Composition(x) m/o	Activation energy (eV) from conductivity plots		Activation energy (eV) from relaxation.
	(intrinsic)	(extrinsic)	
0	1.33	0.92	1.27
5	0.96		0.96
10	0.93		1.10
20	0.95		0.95
30	1.15		1.22
50	0.82		0.89
70	1.40	0.82	0.89
100	1.38	0.85	0.95

3.8 Effect of Milling on Activation Energy

It is observed that the ball-milled samples not only exhibit a higher conductivity but also a lower activation energy for conduction. The activation energies for the ionic conduction are found to have decreased for 20,30 and 50m/o Li_2S compositions after milling processing. This kind of behavior has also been reported in the literature. M. Tatsumisago and co-workers reported that the activation energies for conduction decreases from 78 to 32 kJ mol^{-1} with an increase in milling period for $\text{Li}_2\text{S-SiS}_2\text{-Li}_4\text{SiO}_4$ system.^[27]

As shown in Fig. 3.11-3.13, this decrease in activation energy (slope of curve) for conduction is more for 20 and 30m/o Li_2S compositions as compared to that for 50m/o Li_2S composition. Table 3.5 summarizes the activation energies of various samples before and after milling processing.

Table 3.5: Activation energies before and after milling

Composition(x) m/o Li_2S	Duration of milling hours	Activation energy (E_a) of ordinary sample eV	Activation energy (E_a) of milled sample eV
20	135	0.95	0.68
30	188	1.15	0.72
50	71	0.82	0.76

3.9 Activation Energy-A Comparison(Milled Samples)

The comparison of the activation energies obtained from two different approaches has been carried out for the milled samples of the compositions 20,30 and 50m/o Li_2S . These activation energies are given in Table 3.6

It is clear that that there is no appreciable difference in the activation energies obtained from the conductivity and the dielectric studies for all the three milled samples. It supports the conclusion drawn earlier for conventionally prepared (using solid state reaction method) that only a single conductivity relaxation process is the dominant mechanism in $\text{Li}_3\text{PO}_4\text{-xLi}_2\text{S}$ system.

Table 3.6: Comparison of activation energies obtained from temperature dependence of conductivity and relaxation frequency plots for milled $\text{Li}_3\text{PO}_4\text{-xLi}_2\text{S}$ system

Composition(x) m/o Li_2S	Activation energy from conductivity plots eV	Activation energy (eV) from relaxation plots eV
20	0.68	0.64
30	0.72	0.66
50	0.82	0.76

Lastly, it should be pointed out that the ball-milled samples in general exhibit a higher conductivity and lower activation energy, and most importantly were very stable and their conduction characteristics highly reproducible.

References:

- [1] Sujata T., Ion Conducting Materials: Theory and Application. (2001, Narosa Publishing house) 1
- [2] S. Chandra, Superionic solids: Principles and Applications (1981, North-Holland Publishing company)
- [3] C.A.C. Sequeira and A. Hooper, Solid State Batteries (1985, Martinus Nijhoff Publishers), 19
- [4] C. Julien and G.A. Nazri, Solid State Batteries: Materials design and optimization (1994, Kluwer Academic Publishers), 135-157
- [5] Rotner and Nitzen, Solid State Ionics **28-30** (1988), 3
- [6] Mundy and Jin, Solid State Ionics **21**, (1986), 305
- [7] Mundy and Jin, Solid State Ionics **24** (1987), 263
- [8] N. Lakshmi and S. Chandra, Ion Conducting Materials: Theory and Applications (2001, Narosa Publishing house) 149
- [9] K. Shahi and J.B. Wagner Jr., Solid State Ionics, **3-4** (1981), 295
- [10] K. Shahi and J.B. Wagner Jr., J. Phys. Chem. Solids **44** (1983), 89
- [11] J.R. Macdonald and J.A. Garber, J. Electro-Chemical society, **124** (1997), 1022
- [12] Wanqing Cao and Rosario Gernardt, Solid State Ionics, **42** (1990), 213
- [13] Sujata Chalanobis, PhD. Thesis, IIT Kanpur (1992), 35
- [14] J.E. Bauerle, J. Phys. Chem. Solids, **30** (1969), 2657
- [15] B.a. Boukamp, Solid State Ionics, **18/19** (1986), 136-140
- [16] Ian.D. Raistric, Solid State Ionics **18&19** (1986), 40-49
- [17] J. Ross Macdonald, Impedance Spectroscopy: Emphasizing Solid Materials and Systems (1987), 77
- [18] D. Ravaine and Souquet Comptes Rendus acad. Sci., (Paris 1973), 277C
- [19] R. Matsui, Solid State Ionics, **18/19** (1986), 888-891
- [20] A. Dalvi and K. Shahi, Ion Conducting Materials: Theory and applications Ed. A.R. Kulkarni and P. Gopalan, Narosa Publications (2001), 163

- [21] M. Tanchez, J.P.Malugani, R.Mercier and G. Robert, Solid state Ionics **14**(1984)184
- [22] B. Schoch, E. Hartmann, W. Weppner, Solid state Ionics **18&19**(1986), 531
- [23] M.B.M. Mangion and G.P. Johari, Physics and chemistry of Glasses vol.29,No.6(1988),227
- [24] M.C.R. Shastri and K.J. Rao, Solid Satiare Ionics **44**,(1991),189
- [25] C.T. Moynihan, L.P. Boesch and N.L. Laberge, Physics and Chemistry of Glasses,vol.14,No.6(1973), 122
- [26] V. Provenzano, L.P.Boesch, V.Volterra,c.T.Moyniham and P.B.Macedo, The Journal of the American Ceramic Society, vol.55, no.10(1972),492
- [27] M. Tatsumisago, H. Morimoto, H. Yamashita, T. Minami, Solid State Ionics **136-137**, (2000), 486

133680
Date Slip

[illegible]